Developmental Biology 380 (2013) 243–258

Contents lists available at SciVerse ScienceDirect

Developmental Biology

journal homepage: www.elsevier.com/locate/developmentalbiology

Xenopus laevis nucleotide binding protein 1 (xNubp1) is important for convergent extension movements and controls ciliogenesis via regulation of the actin cytoskeleton ☆

Andriani Ioannou, Niovi Santama, Paris A. Skourides *

Department of Biological Sciences, University of Cyprus, Nicosia 2109, Cyprus

ARTICLE INFO

Article history:
Received 21 December 2012
Received in revised form
24 April 2013
Accepted 7 May 2013
Available online 16 May 2013

Keywords:
Nubp1
Ciliogenesis
Actin
Basal bodies
Convergent extension
Xenopus

ABSTRACT

Nucleotide binding protein 1 (Nubp1) is a highly conserved phosphate loop (P-loop) ATPase involved in diverse processes including iron–sulfur protein assembly, centrosome duplication and lung development. Here, we report the cloning, expression and functional characterization of *Xenopus laevis* Nubp1. We show that xNubp1 is expressed maternally, displays elevated expression in neural tissues and is required for convergent extension movements and neural tube closure. In addition, xNubp1knockdown leads to defective ciliogenesis of the multi-ciliated cells of the epidermis as well as the monociliated cells of the gastrocoel roof plate. Specifically, xNubp1 is required for basal body migration, spacing and docking in multi-ciliated cells and basal body positioning and axoneme elongation in monociliated gastrocoel roof plate cells. Live imaging of the different pools of actin and basal body migration during the process of ciliated cell intercalation revealed that two independent pools of actin are present from the onset of cell intercalation; an internal network surrounding the basal bodies, anchoring them to the cell cortex and an apical pool of punctate actin which eventually matures into the characteristic apical actin network. We show that xNubp1 colocalizes with the apical actin network of multiciliated cells and that problems in basal body transport in xNubp1 morphants are associated with defects of the internal network of actin, while spacing and polarity issues are due to a failure of the apical and sub-apical actin pools to mature into a network. Effects of xNubp1 knockdown on the actin cytoskeleton are independent of RhoA localization and activation, suggesting that xNubp1 may have a direct role in the regulation of the actin cytoskeleton.

Introduction

Vertebrate embryonic development is a highly dynamic and complex process. Many distinct, yet interconnected cellular events, must take place in concert in order to produce a fully functional and viable organism. For vertebrate embryos to develop normally, they must undergo coordinated changes in cell fate and cell movements (Wallingford, 2006). During convergent extension (CE), a morphogenetic cell movement which is vital during embryonic development, cells narrow along one axis and elongate along a perpendicular axis, in order to correctly elongate the body axis and close the neural tube (Antic et al., 2010; Wallingford et al., 2002; Wallingford and Harland, 2001). During neurulation, presumptive hindbrain and spinal cord undergo CE movements in parallel to similar events occurring in the underlying mesoderm. Abnormal CE movements during the formation of the neural tube lead to neural tube defects (NTDs) such as anencephaly, craniorachischisis and spina bifida (Wallingford, 2006). Defects in neural tube closure are the second most common birth defect in humans (Antic et al., 2010; Wallingford, 2005, 2006). At the molecular level, experiments performed in *Xenopus* and *Zebrafish* have demonstrated that the non-canonical Wnt pathway or planar cell polarity (PCP) pathway, mediated by Dishevelled, plays a crucial role in the establishment of cell polarity (Smith et al., 2000; Tada and Smith, 2000; Wallingford et al., 2000). The PCP pathway is also required for convergent extension, and interestingly several PCP pathway members have also been linked to ciliogenesis (Park et al., 2006, 2008; Stubbs et al., 2008; Wallingford, 2006; Wallingford and Mitchell, 2011).

Cilia are microtubule-based organelles, extending from basal bodies on the surface of most vertebrate cells. There are two main types of cilia; primary and motile cilia. Primary cilia can be found

* Corresponding author.
E-mail addresses: Ioannou.andriani@ucy.ac.cy (A. Ioannou), Santama@ucy.ac.cy (N. Santama), skourip@ucy.ac.cy (P.A. Skourides).

0012-1606/$ - see front matter © 2013 The Authors. Published by Elsevier Inc. All rights reserved.
http://dx.doi.org/10.1016/j.ydbio.2013.05.004

on almost every cell type; they are short, immotile and play an important role in sensing mechanical and chemical stimuli. Motile cilia are restricted to more specialized epithelia which are essential for generating fluid flow along their surface. These include, but are not restricted to; the airways, the ventricles of the brain and the oviducts. Motile cilia are typically much longer than primary cilia and can be found in single copy as motile mono-cilia or multicilia (Goetz and Anderson, 2010; Pazour and Witman, 2003; Pedersen et al., 2008; Roy, 2009). Disruption of cilia function or ciliogenesis can lead to a variety of human diseases or "ciliopathies" as they have been recently coined (Baker and Beales, 2009; Hildebrandt et al., 2011; Wallingford and Mitchell, 2011; Zariwala et al., 2007).

In multi-ciliated cells, basal bodies form de novo deep within the cytoplasm (Sorokin, 1968). The transport of these basal bodies to the apical surface and their subsequent docking occurs via an actin-myosin based mechanism (Boisvieux-Ulrich et al., 1990; Dawe et al., 2007; Klotz et al., 1986; Lemullois et al., 1987). The apical surface of multi-ciliated cells is enriched with a dense meshwork of actin. The actin regulators RhoA and Ezrin, in addition to planar cell polarity (PCP) pathway proteins Dishevelled, Inturned and Fuzzy have been shown to be important for the apical enrichment of actin and basal body docking (Gomperts et al., 2004; Huang et al., 2003; Pan et al., 2007; Park et al., 2006, 2008). In *Xenopus laevis* ciliated epidermal cells, this network of actin comprises two distinct but interconnected pools; the apical and sub-apical pools of actin (Werner et al., 2011). Loss of the apical actin network leads to problems with basal body localization and polarity and appears to be necessary for basal body docking (Boisvieux-Ulrich et al., 1990; Park et al., 2006, 2008; Werner et al., 2011). The formation of the apical actin network is temporally linked to basal body docking and is dependent on RhoA (Hall, 1998; Pan et al., 2007). Once basal bodies dock at the apical surface, they must be polarized in order for the cilia to beat in a synchronized manner and create directional fluid flow. The sub-apical actin network has been shown to be important for basal body cell-wide polarity in addition to basal body spacing (Boisvieux-Ulrich et al., 1985; Frisch and Farbman, 1968b; Mitchell et al., 2009; Werner et al., 2011). Planar polarization of ciliary beating is initially weak and becomes refined by a flow mediated positive feedback mechanism (Mitchell et al., 2007). In ciliated *X. laevis* epidermal cells, the basal bodies are polarized along the anterior–posterior axis in the direction of the effective stroke; which is posterior with a ventral bias (Mitchell et al., 2007,2009; Park et al., 2008). The basal foot, an accessory structure of the basal body, points in the direction of ciliary beat (the effective stroke) (Boisvieux-Ulrich et al., 1991; Frisch and Farbman, 1968a) and the striated rootlet points in the opposite direction (Boisvieux-Ulrich et al., 1991; Mitchell et al., 2007, 2009; Park et al., 2008). Although much has been discovered concerning ciliogenesis in multiciliated epithelia, the precise mechanisms involved in basal body migration, docking and polarity are not yet clear.

Nucleotide binding protein 1 (Nubp1) is a phosphate loop (P-loop) ATPase which is highly conserved from yeast to humans. P-loop protein subgroups perform an array of functions, examples of which include; translation, signal transduction, protein transport and localization, chromosome partitioning and cell division, metal ion insertion and membrane transport (Hausmann et al., 2005; Leipe et al., 2002). Nubp1 proteins are evolutionary well conserved among eukaryotes, are ubiquitously expressed throughout embryogenesis and in many adult organs (Nakashima et al., 1999) and are essential for cell viability (Hausmann et al., 2005; Leipe et al., 2002; Vitale et al., 1996). Nubp1 was initially characterized as a scaffold in the iron–sulfur protein assembly process (Hausmann et al., 2005; Netz et al., 2007; Stehling et al., 2008). Sequence analysis also revealed structural homology between Nubp1 and the Mrp/NBP35 family of NTPases which are involved in the cell division process and chromosome partitioning (Koonin, 1993; Lutkenhaus and Sundaramoorthy, 2003; Nakashima et al., 1999; Shahrestanifar et al., 1994; Vitale et al., 1996). In mouse cells, Nubp1 has been shown to interact with Nubp2, an Mrp/NBP35 NTPase with high sequence similarity to Nubp1, and both proteins to also interact with minus-end directed motor protein KIFC5A. Nubp1, Nubp2 and KIFC5A have been implicated in the regulation of centriole duplication with their depletion causing supernumerary centrioles (Christodoulou et al., 2006). Interestingly, a proteomic study using *Chlamydomonas reinhardtii* has revealed Nubp1 as a flagellar protein (Pazour et al., 2005). A very recent paper has shown that murine Nubp1 is essential for normal embryonic development. Schnatwinkel and Niswander (2012) show that a mutated form of Nubp1, which differs only in two amino acids at its C-terminus, causes lung hypoplasia leading to death shortly after birth, syndactyly and eye cataracts (Schnatwinkel and Niswander, 2012).

Here we describe the molecular cloning and functional characterization of *X. laevis* Nubp1 and report that xNubp1 is expressed throughout embryonic development in a number of tissues, shows elevated expression in neural tissues and is essential for normal embryonic development. Knockdown of xNubp1 results in phenotypes associated with problems in CE and defective ciliogenesis; such as disruption of neural tube closure and anterior–posterior (AP) axis elongation, aberrant basal body migration and docking as well as defects in left–right patterning. Finally, we show that loss of xNubp1 elicits these effects on ciliogenesis through Rho independent destabilization of the actin cytoskeleton.

Material and methods

Embryo manipulations

Female adult *X. laevis* were ovulated by injection of human chorionic gonadotropin. Eggs were fertilized *in vitro*, dejellied in 2% cysteine (pH 7.8) and subsequently reared in 0.1x MMR (Marc's modified ringers) and staged according Neiuwkoop and Faber (Nieuwkoop, 1994). For microinjections, embryos were placed in a solution of 4% Ficoll in 0.33x MMR and injected using a glass capillary pulled needle, forceps, a Singer Instruments MK1 micromanipulator and Harvard Apparatus pressure injector. After injections, embryos were reared for 2 h or until stage 8 in 4%Ficoll in 0.33x MMR and then washed and maintained in 0.1x MMR alone. Capped mRNA was in vitro transcribed using mMessage machine kits (Ambion). For all experiments we injected morpholinos at 4 to 46 ng per blastomere and mRNAs at various amounts. For most experiments, injections were made into either the ventral blastomeres to target the epidermis or the dorsal blastomeres to target neural or mesodermal tissue at the 4-cell stage. Embryos were allowed to develop to the appropriate stage and then imaged live, dissected or fixed in MEMFA (Sive et al., 2010) for 1–2 h at room temperature (RT). Fixed embryos were either used immediately or serially dehydrated in methanol and stored at −20 °C. For Live imaging, embryos were anesthetized in 0.01% benzocaine in 0.1 MMR.

Isolation of stage 31 tailbud skin for RT-PCR was carried out as follows: tailbuds were dissected into three regions (RT-PCR was carried out on all three regions separately) in order to separate the regions of the embryos which were shown by ISH to express high amounts of xNubp1. The anterior region which contained the head, branchial arches and pronephros was removed and the dorsal region containing the neural tube, notochord, somites and tailbud were then removed. The skin surrounding the remaining ventral/belly region was then carefully peeled from the endoderm.

Cloning and RT PCR

cDNA was prepared via reverse transcription (SuperScriptIII First strand synthesis, Invitrogen) from RNA extracted (using standard protocol) from *X. laevis* embryos. We then amplified xNubp1 by standard PCR (list of primers found in Supplementary Table 1). The xNubp1 and xNubp2 PCR fragments were then cloned into the SalI–XbaI sites of the pCS108 vector. The clones were then verified by sequencing and then using the verified pCS108-xNubp1 vector, we constructed the various tagged and untagged versions of the xNubp1 constructs. For RT-PCR, cDNA was synthesised using the same method mentioned above for different developmental stages and different tissues. The PCR was carried out using specific primer pairs. The PCR products were run on a 1–1.5% agarose gel and images were captured using UVP iBox imaging system.

Cloning of introns and design of splice blocking antisense morpholinos

Introns in xNubp1 were identified first by comparing cDNA sequence to the *Xenopus tropicalis genome* sequence and then the analogous primers were designed (Supplementary Table 1). *X. laevis* Nubp1 genomic DNA, including the intronic regions, was then amplified by PCR, cloned into the CS108 vector and sequenced. Splice-blocking antisense morpholino oligonucleotides (MOs) were designed and ordered from Gene Tools, LLC. To determine the effectiveness of the splice disruption by the MO, RNA was extracted from MO-injected and control embryos and cDNA was prepared using the Superscript™ kit (Invitrogen). PCR was then performed using the same primers used for amplifying the intronic regions.

In situ hybridization

Whole-mount in situ hybridization of *Xenopus* embryos was performed according to Smith and Harland (1991). Probes used were: xNubp1, Sox2, Chrd, MyoD, Pax3, Pax6, N-Tub, Twist, Pitx2c, Xnr1. Bright field images were captured on a Zeiss LumarV12 fluorescent stereomicroscope.

Immunohistochemistry

Stored embryos were rehydrated by serial washes. Embryos were then permeabilized in PBDT (1 × PBS+0.5% Triton-X100+1% DMSO) for several hours at RT. Embryos were then blocked in PBDT+1% normal goat serum for 1 h at RT. Primary antibodies were then added (in block solution): rabbit polyclonal or mouse monoclonal Anti-GFP (1:500–1000 Invitrogen), mouse monoclonal Anti-acetylated tubulin (1:500–1000, Santa Cruz Biotechnology), and mouse monoclonal Zo-1 (1:500–1000 Invitrogen), and embryos were incubated for 4 h at RT or overnight at 4 °C. The next day, embryos were washed 4 × 10 min in PBDT. Embryos were then incubated in secondary antibodies: anti-mouse or rabbit Alexa 633, alexa 488 (from Invitrogen), anti-mouse or rabbit Cy3(from Jackson Immunoresearch) and Alexa-fluor 488 Phalloidin (Invitrogen) at 1:500–1000 dilution at RT for 1–2 h and then washed 4 × 10 min in PBDT again. Embryos were then post-fixed in MEMFA for 15–30 min at RT, washed in 1 × PBS, imaged immediately or dehydrated in methanol and cleared in a 2:1 mixture of BB:BA (Benzyl benzoate:Benzyl alcohol). The embryos were imaged on a Zeiss LSM 710 laser scanning confocal microscope and Zen 2010 software or a Zeiss Axio Imager Z1 using a Zeiss Axiocam MR3, the Axiovision software 4.7.

Western blots

Protein lysates were prepared by homogenizing embryos in ice cold MK's modified lysis buffer (50 mM Tris pH 8.0, 150 mM NaCl, 0.5%NP-40, 0.5% Triton-X100, 100 mM EGTA, 5 mM NaF) supplemented with protease inhibitors. Embryos were homogenised by pipetting up and down. Homogenates were then cleared by centrifugation at 15,000 × *g* for 15–30 min at 4 °C. Proteins (usually ½–1 embryo equivalents) were run on an SDS-page gel and then blotted onto a PVDF membrane. Blots were then blocked in 5% milk in TBSTw (1 × TBS buffer +0.1%Tween-20). Blots were incubated with primary antibodies in 5% milk overnight at 4 °C. Antibodies used: goat polyclonal Anti-Nubp1 (1: 500–1000, Santa Cruz Biotechnology), rabbit polyclonal Anti-actin (1:1000 Santa Cruz Biotechnology). Visualization was performed using HRP-conjugated antibodies (Santa Cruz Biotechnology anti-rabbit, mouse and goat) and detected using the Lumisensor chemiluminescent reagent kit (Genscript).

Fluid flow

For the assessment of fluid flow, 31/32 stage embryos were anaesthetized in 0.01% benzocaine and placed in silicone grease (High Vacuum Grease, Dow Corning) wells on glass slides with a clover glass on top. Quantum dots of 655 nm (QTracker non-target QDs, Invitrogen) were then added to the media. We carried out time-lapse microscopy using the Zeiss Axio Imager Z1 using a Zeiss Axiocam MR3, the Axiovision software 4.7.

Transmission electron microscopy

Electron microscopy was done essentially as described by Steinman (1968). Briefly, embryos were fixed in 2.5% phosphate-buffered gluteraldehyde over-night at 4 °C and then post-fixed in 1% phosphate-buffered osmium tetroxide for 1 h at room temperature. The embryos were then dehydrated in a graded series of ethanol. Embryos were then washed in propylene oxide and embedded in epoxy resin. Embedded embryos were sectioned (60–70 nm) and sections were mounted on copper grids, counter stained with uranyl acetate and lead citrate and imaged in the TEM (Jeol, JEM 1010).

Gastrocoel roof plate assay

Embryos were fixed in MEMFA at stage 17. The GRP was then manually dissected and post fixed for a further 15 min. GRP tissue was then used for immunofluorescence as described above.

Fluorescence recovery after photobleaching (FRAP)

The FRAP experiments were conducted using a laser scanning confocal microscope (Zeiss LSM 710). Stage 27–29 mKate2-actin expressing or mKate2-actin and Centrin2-YFP expressing embryos were anaesthetized in 0.01 % Benzocaine in MMR and immobilized in silicone grease wells on glass slides. A small area of an mKAte2-actin positive epidermal cell was imaged (11.5 μm × 11.5 μm) using a Plan-Apochromat 63x/1.40 Oil DIC M27 objective lens (Zeiss) and a 543 nm laser was used both during acquisition (2.8%) and bleaching (100%). Emission of mkate2 was detected between 572 and 754 nm. A total of 30 of frames were acquired at 5 s intervals. Two frames were acquired as a pre-bleaching control, the region of interest (rectangular region roughly 4 × 5 μm) was bleached within one frame, and the fluorescence recovery was measured in frames 4–30. In order to obtain full recovery rates for control ciliated cells the interval between acquired frames was changed to 20 s for the 11–30th frames. The Zeiss Zen 2010 software was used

for FRAP analysis. The fluorescence recovery curve was fitted by single exponential function, given by: $F(t)=A(1-e^{-R})+B$; where $F(t)$ is the intensity as time t; A and B are the amplitudes of the time-dependent and time-independent terms, respectively; τ is the lifetime of the exponential term (time constant), and the recovery rate is given by $R=1/\tau$.

Results

Cloning of Xenopus laevis nucleotide binding protein 1

First strand cDNA was reverse transcribed from gastrula stage *X. laevis* mRNA. Primers were designed based on the provisional sequences of *X. laevis* Nubp1a and Nubp1b from www.xenbase.org (XB-GENE-992731 and XB-GENE-6252195) (Bowes et al., 2010) and the NCBI database (GenBank: 494723 and 496286) and used to amplify the coding and untranslated regions of xNubp1-a and xNubp1-b paralogs, respectively and clone them into the pCS108 vector. Sequenced clones were identical to the provisional sequences from Xenbase and NCBI (Supplementary Fig. 1). The xNubp1 paralogs had very few minor amino acid differences (96% sequence identity) (Supplementary Fig. 1B); therefore, only xNubp1a was used to generate most of the constructs.

Spatial and temporal developmental expression of xNubp1

The temporal expression pattern of xNubp1 was examined by RT-PCR from oocytes and stage 8 to 34 embryos. xNubp1 expression was present at all stages (Fig. 1A), indicating that xNubp1 is a maternal gene and is expressed throughout early development. During gastrulation, xNubp1 showed elevated expression in the animal hemisphere (Fig. 1Bi). During neurulation, elevated xNubp1 expression was observed in the neural plate (stage 19) (Fig. 1Bii) and at stage 22 expression expanded to the streaming cranial neural crest cells, the neural fold, the developing eye and to a small extent in the epidermis (Fig. 1Biii). By stage 29/30, xNubp1 expression was observed in the otic placodes, developing eye, branchial arches, neural tube, heart anlage, pronephros and also weakly in the epidermis and somites (Fig. 1Biv). These data show that xNubp1 is expressed throughout development in various tissues and its expression is elevated in neural tissues, which suggest a possible involvement of xNubp1 in neural development.

Gain and loss-of-function of xNubp1

Overexpression of xNubp1 did not lead to any developmental phenotypes (data not shown). In order to explore the role of Nubp1 in *Xenopus* development further, we carried out loss of function experiments using antisense morpholino oligonucleotides (MOs). To deplete xNubp1 at the protein level, we designed three distinct morpholinos (MO1, MO2 and SpMO). Two of the three xNubp1 MOs were translation blocking MOs targeting separate areas of the xNubp1 mRNA. xNubp1–MO1 targeted a sequence identical to both xNubp1 pseudo-alleles (xNubp1a and xNubp1b) and xNubp1–MO2 targeted a sequence which was not identical to both pseudo-alleles and was more effective against xNubp1a mRNA (Supplementary Table 2). We also obtained a general control MO (CoMO) and designed an xNubp1 specific 5-base pair mismatch control MO (mmMO) (Supplementary Table 2). We tested the efficiency of the translation blocking MOs by co-injection of the MOs with an xNubp1 surrogate containing the sequence recognized by the MOs (Supplementary Fig. 2A and B). The third MO (SpMO) was a splice blocking MO which targeted the exon1- intron1 splice junction of xNubp1 pre-mRNA. This led to an intron inclusion of intron1 (94 base pairs) which in turn led to a premature stop codon. The efficiency of this morpholino was examined using RT PCR. Morphant embryos retained xNubp1 intron 1 (Supplementary Fig. 2C). At high amounts of SpMO (68 ng) the correctly spliced xNubp1 transcript is entirely absent (Supplementary Fig. 2C). Embryos injected with more than 60 ng of any of the three MOs but not the CoMO or mmMO died before completing neurulation (data not shown) which is in agreement with previous studies showing that Nubp1 is required for cell survival (Hausmann et al., 2005; Schnatwinkel and Niswander, 2012; Vitale et al., 1996).

xNubp1 Is involved in convergent extension and neural tube closure

Due to the elevated expression levels of xNubp1 in neural tissues, we initially targeted the MOs into the 2 dorsal blastomeres at the 4 cell stage. xNubp1 morpholino injected embryos (morphants) began showing dose dependent developmental defects from the onset of neurulation. Morphants from all three MOs (10–25 ng) exhibited delays and defects in neural tube closure (95%; $n=60$) (Fig. 2A) and had shortened trunks (shorter along the anterior–posterior axis) (100%; $n=73$) (Fig. 2B and C). Although the neural tube did eventually close in most xNubp1 morphants, roughly 8% ($n=60$) of morphant embryos displayed a failure of posterior neural tube closure (Spina bifida) leading to an

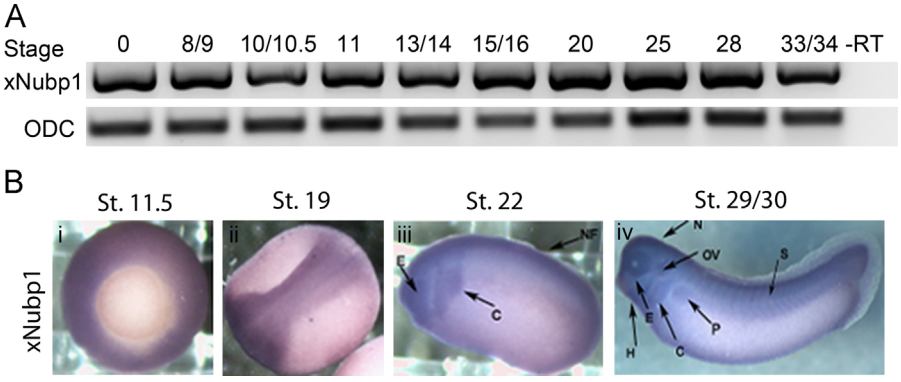

Fig. 1. xNubp1 is a maternal gene expressed throughout development. (A) RT-PCR of different stages of *Xenopus laevis* embryonic development. xNubp1 is expressed at all stages of embryonic development tested. (B) Whole-mount in situ hybridization to detect xNubp1 expression. (Bi) xNubp1 is expressed in the animal hemisphere. (Bii) xNubp1 expression is elevated in the neural plate. (Biii) Stage 22 embryos show expression in the neural folds [NF], presumptive eye [E] and neural crest cells [C]. (Biv) In stage 29/30 tailbuds, xNubp1 is expressed in the otic vesicle [OV], the eye, the branchial arches [B], neural tube [N], heart anlage [H] the pronephros [P] and also weak epidermal and somitic [S] expression is visible.

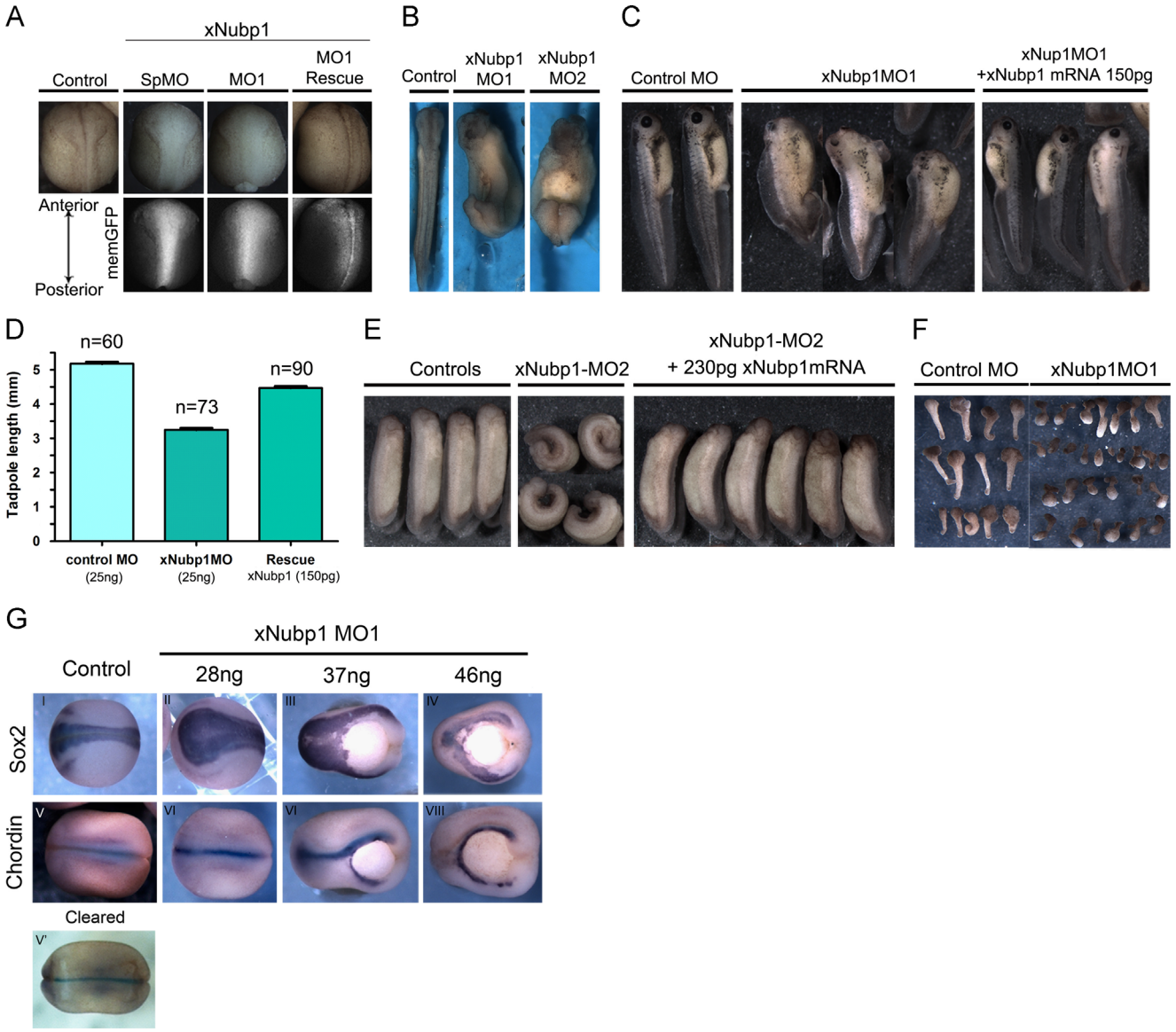

Fig. 2. xNubp1 knock-down causes failure of neural tube closure and other CE related phenotypes but does not affect cell specification. (A) Dorsal view of stage 19/20 embryos injected in the dorsal blastomeres at the four cell stage. xNubp1 SpMO (17 ng) and MO1 (25 ng) injected embryos show a delay in neural tube closure and an open neural plate. Co-injection of MO1 (25 ng) with 200 pg xNubp1 mRNA rescued neural tube closure delay. (B) Dorsal view of a stage 28 uninjected control embryo, xNubp1–MO1 and MO2 injected embryos (~35 ng). Morphants have an open back due to posterior neural tube closure failure. (C) xNubp1–MO1 (~25 ng) tadpoles have a shortened axis. Co-injection of xNubp1 mRNA partially rescues the shortened axis. (D) Bar chart showing the average length of Stage 37/38embryos from three separate experiments. Error bars indicate standard error of the mean (SEM). Control embryos had mean length of 5.18 ± 0.046 mm, morphants displayed a mean length of 3.24 ± 0.05 mm and rescues showed a mean length of 4.47 ± 0.046 mm. (E) Injection of xNubp1 MO2 (15 ng) in 1 of 4 dorsal blastomeres leads to curved embryos. This can be rescued by co-injection with xNubp1 mRNA. (F) xNubp1 MO1 and CoMO (25 ng) injected caps induced with activin. xNubp1 MO injected caps do not elongate as well as controls. (G) Control and morphant embryos processed by whole mount in situ hybridization to visualize Sox2 and chordin expression. (G II–IV) *Sox2* is expressed in morphants with varying concentrations of MO; however, neural plates are significantly wider than in controls. (G V–VIII) Chordin is expressed in all morphant embryos; however the staining appears more intense due to fact that chordal mesoderm is exposed due to the open neural tube.

open-back phenotype (Fig. 2B). The frequency of this phenotype increased (15–20%; $n=50$) at higher amounts of MO (25–35 ng). At these amounts, we also observed embryos which lacked some anterior structures (20%; $n=50$) (Fig. 2C). The neural tube closure and axis elongation phenotypes were suggestive of a defect in convergent extension (CE). These defects could be partially rescued by co-injection of xNubp1 mRNA with MOs (Fig. 2A, C–E), suggesting that the phenotypes were specific and induced due to loss of xNubp1. Embryos injected on one side curved towards the side of injection (75.5%, $n=80$) (Fig. 2E middle panel), which also pointed to a problem with CE. Co-injection of xNubp1 mRNA with MOs also rescued the curved embryo phenotype (Fig. 2E, last panel). 80% of the embryos were no longer curved, roughly 16% had a slight curve and only about 4% of the embryos were not rescued ($n=122$). As mentioned above, all three MOs induced very similar phenotypes, while the two control MOs did not elicit any phenotype (Fig. 2C, D and F; Supplementary Fig. 2E), providing further evidence that the phenotype was specific. In order to determine whether CE was in fact affected by the depletion of xNubp1, we conducted an in vitro elongation assay. We observed that morphant caps did not undergo convergent extension to the same degree as control caps (Fig. 2F). Overall, these data suggest that the loss of xNubp1 leads to convergent extension related defects.

In order to examine if the developmental defects elicited by the morpholinos were due to problems with cell fate specification, we

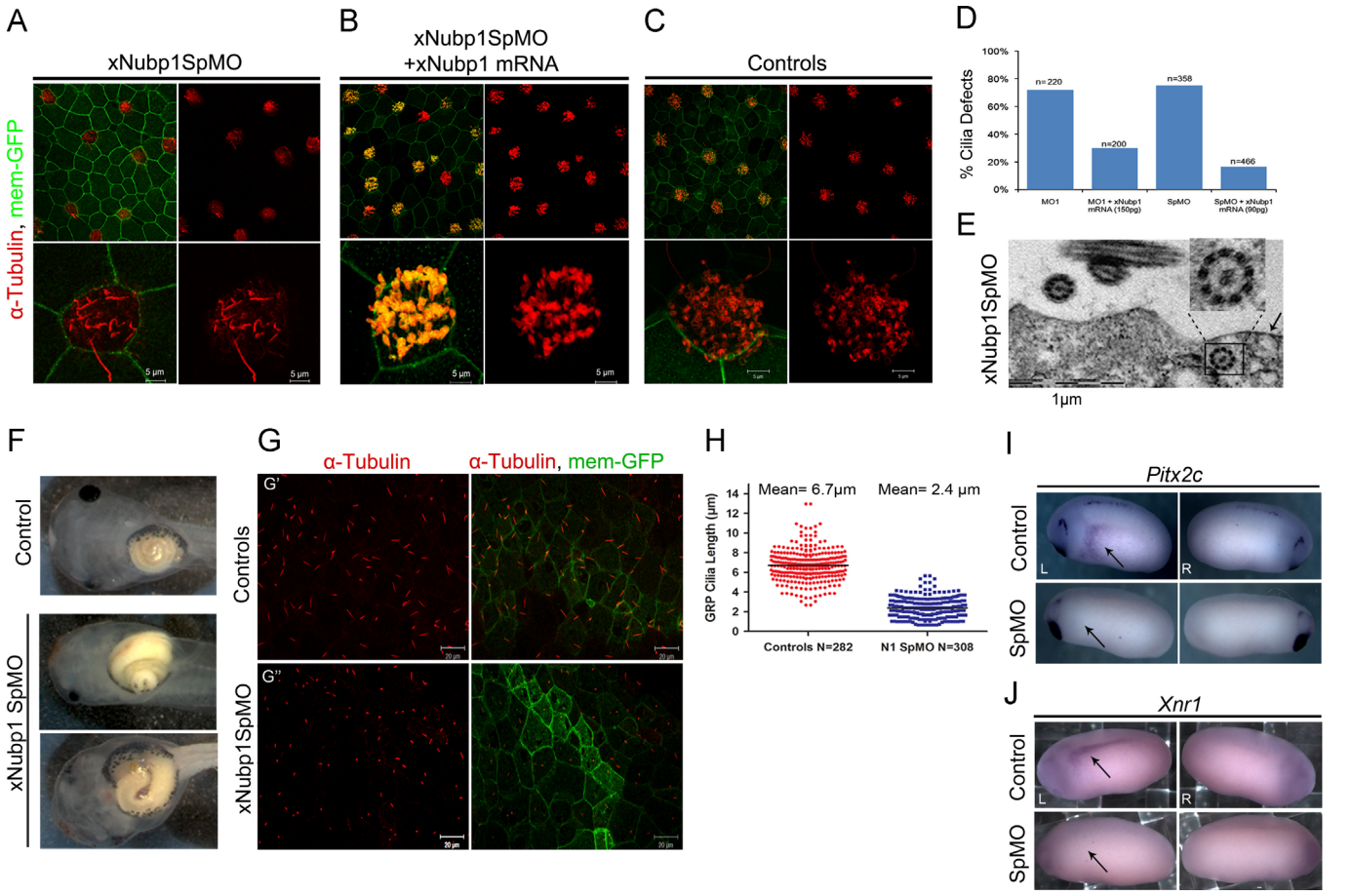

Fig. 3. Knockdown of xNubp1 leads Ciliogenesis defects. ((A)–(C)) Immunofluorescence data showing surface views of ciliated epidermis from intact embryos. (A) xNubp1 SpMO (13 ng) morphant embryo, showing mainly internal acetylated α-tubulin positive structures. Very few cilia project outward from the apical surface. (B) Co-injection of xNubp1 SpMO with xNubp1 mRNA (90pg) rescues the phenotype and confirms the specificity of the MO. (C) Control epidermis showing normal ciliated cells. (D) Quantification of ciliated cells which lack cilia and have internal acetylated tubulin positive structures. Co-Injection of xNubp1 mRNA with either xNubp1MO1 or SpMO partially rescues cilia phenotype (E) TEM of cross section from stage 31 tailbud injected with xNubp1–SpMO, showing an internal ciliary axoneme right below the apical surface (black arrow). (F) Ventral view of *X. laevis* tadpoles. Unlike control embryos, xNubp1 morphants have various gut looping defects. (G) Maximum intensity projection (MIP) of optical sections from immunostaining showing cilia projecting out from posterior apical surface of a normal GRP (G′) and shorter cilia projecting for the apical surface of a SpMO morphant GRP (G″). In some morphant cells the cilia remain centrally localized and have not migrated to the posterior side of the cell. (H) Average length of GRP cilia is significantly reduced in xNubp1 morphants (2.4 ± 0.06 µm) compared to controls (6.7 ± 0.1 µm). Horizontal lines indicate the mean, Vertical line SEM, $p < 0.0001$ Mann–Whitney test. ((I)–(J)) *Pitx2c* and *Xnr1* expression at stage 24. (I) In wild type embryos Pitx2c is expressed in left lateral plate mesoderm (LPM) (black arrow). In xNubp1 morphants *Pitx2c* is absent. (J) *Xnr1* expression is also lost from in xNubp1 morphants (black arrow, bottom panel).

carried out whole mount in situ hybridization (WISH) on MO injected and control embryos. We used probes against Sox2, a pan-neural marker, chordin, a marker for the chordal mesoderm (Fig. 2G) and several other markers such as MyoD, Pax3, N-tub Twist and Pax6 (Supplementary Fig. 3; data not shown). These experiments showed that both neural and mesodermal specification were unaffected in morphant embryos and suggested that the observed morphogenetic defects were not due to changes in either mesodermal or neural patterning (Fig. 2G I–VIII; Supplementary Fig. 3). In addition, from the in situ experiments it also became clear that the neural plate in morphant embryos was indeed wider than that of control embryos, confirming the effects of xNubp1 down regulation on neural tube closure (Fig. 2GII).

xNubp1 Is involved in ciliogenesis in the Xenopus laevis epidermis and gastrocoel roof plate

When we used MOs to block xNubp1 translation or splicing in ventral tissues, we observed that xNubp1 morphants failed to undergo the characteristic drifting motion caused by beating of the cilia on multiciliated epidermal cells (data not shown). We therefore went on to investigate whether xNubp1 was required for ciliogenesis in multiciliated epidermal cells. Immunostaining of morphant embryos at stage 29–31 with acetylated tubulin revealed a dose dependent effect on ciliogenesis. With low amounts of MO (5–8 ng), most of the "low-dose" morphant epidermal ciliated cells did project cilia from the apical surface (data not shown), however the embryos still failed to undergo the drifting motion. At slightly higher amounts (8–15 ng), the ciliated epidermal cells in xNubp1 "high-dose" morphants projected fewer and shorter cilia from the apical surface and showed an enrichment of polymerized cytoplasmic acetylated α-tubulin (Fig. 3A, Supplementary Fig. 2H and I). This phenotype was observed with all three xNubp1-MOs but not with control or mismatch MOs (Supplementary Fig. 2F) and could be partially rescued by co-injection with xNubp1 mRNA (Fig. 3B and D). Transmission electron microscopy (TEM) revealed the presence of internal ciliary axonemes (Fig. 3E). Interestingly, preliminary data showed that down regulation of xNubp2 also led to a similar phenotype (Supplementary Fig. 2G). These data show that the down

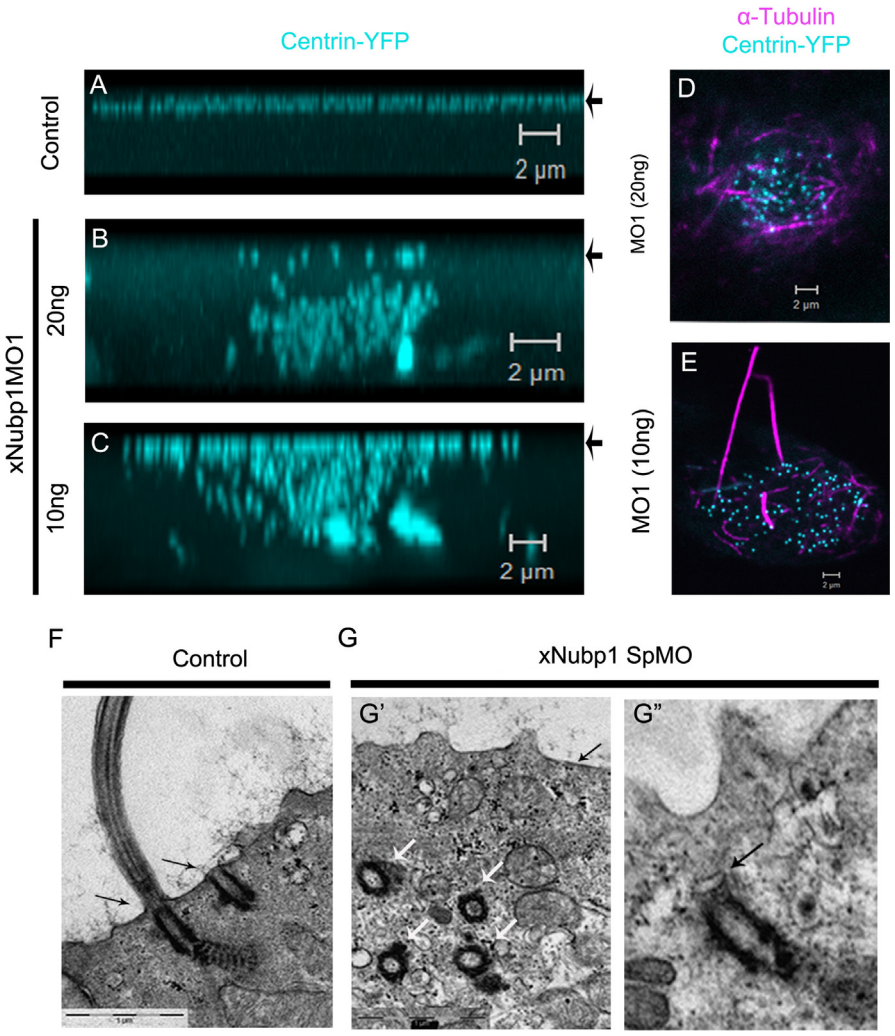

Fig. 4. xNubp1 is required for basal body migration and docking at the apical surface of ciliated epidermal cells. ((A)–(C)) 3D reconstructions from confocal optical sections projected in the *x*–*z* plane with the position of the apical surface indicated by black arrows (A) Centrin2-YFP in control cells is localized at the apical surface of ciliated cells. ((B)–(E)) A dose dependent range of effects on basal body migration is seen in Nubp1 morphants. (B) In high-dose morphant cells, most of the basal bodies fail to reach the apical surface remaining deep within the cell. (C) In cells with an intermediate amount of MO, some me basal bodies do reach the apical surface with most still remaining in the cytosol. (D) Optical section from a xNubp1 morphant ciliated epidermal cell showing internal acetylated tubulin in close association with the basal bodies deep within the cell body. (E) Cells with apically localized basal bodies have polymerized cytoplasmic acetylated α-tubulin just below the apical surface. ((F), (G)) TEM on cross-sections from stage 31tailbuds. (F) In control cells, basal bodies in have migrated and docked to the apical surface (black arrows). (G′) In xNubp1 morphants, basal bodies (white arrows) fail to migrate to the apical surface (black arrow). (G″) Basal body in a xNubp1 morphant cell has migrated to the apical surface but has not docked properly (black arrow).

regulation of xNubp1 leads to defective ciliogenesis in the *X. laevis* epidermis; however, the problem is not due to a failure of axonemal microtubule polymerization.

Due to the fact that WISH did not reveal a high expression of xNubp1 in ciliated cells and our data indicated that xNubp1 is involved in ciliogenesis, we carried out reverse transcription PCR on isolated tailbud skin in order to verify the expression of xNubp1 in the epidermis. RT-PCR verified that xNubp1 was also expressed in the skin (Supplementary Fig. 2D).

The *Xenopus* gastrocoel roof plate (GRP) is a planar polarized monociliated epithelium derived from the superficial mesoderm. It is homologous to the mouse Posterior notochord (PNC, Node) and Kuppfer's vesicle (KV) in teleost fish and contains posterior localized motile cilia which beat in a circular clockwise fashion to create a leftward flow of extracellular material which is required for left–right asymmetry (Blum et al., 2009; Chung et al., 2012; Schweickert et al., 2007). xNubp1 morphants displayed gut development defects when dorsal tissues were targeted. The gut either failed to loop or displayed heterotaxia (Fig. 3F) in morphant embryos (100%, $n=60$). Situs inversus of the gut was difficult to determine due to the fact that in many cases, the positioning/orientation of the gut was affected (Fig. 3F). Since the correct looping of the gut is linked to cilia-driven leftward flow (Blum et al., 2009; Chung et al., 2012; Schweickert et al., 2007), we decided to examine the GRP cilia in xNubp1 morphant embryos in order to determine whether or not xNubp1 had a generalized role in ciliogenesis. We targeted GRP cells by injecting xNubp1MOs into the dorsal marginal zone (DMZ) of two cell stage *X. laevis* embryos, dissecting the GRP tissue at stage 17 and conducting immunostaining against acetylated α-tubulin. We observed that xNubp1 morphant GRP cells had shorter cilia (Mean = 2.4 μm) than control cells (Mean 6.7 μm) (Fig. 3G and H). It was also apparent that many of the cilia of morphant cells were located more centrally (Fig. 3G″) compared to the posterior positioning of cilia of wild-type cells (Fig. 3G′). In order to determine whether left–right asymmetry was disrupted in xNubp1 morphants, we examined the expression of left–right lateralization markers. In control embryos, *Pitx2c* was expressed in the left lateral plate mesoderm (LPM), however, was absent from the right side (100%, $n=30$) (Fig. 3I top panels). When xNubp1 was knocked down, left LPM

expression of *pitx2c* was absent (100%, $n=59$) (Fig. 3I; bottom panels). Similar results were obtained for *xnr1*. Control embryos displayed expression of xnr1 in the left LPM (100%, $n=30$) (Fig. 3J top panels), whereas xNubp1 MO injected embryos lacked xnr1 transcripts in the LPM (100%, $n=33$) (Fig. 3J; bottom panels). These results indicate that xNubp1 is important for regulating GRP ciliogenesis, which in turn is essential for the establishment of left–right asymmetry. The high penetrance of this phenotype, however, may also indicate an additional defect, possibly unrelated to ciliogenesis. Taken together, these data show that xNubp1 is important for ciliogenesis in multiciliated as well as monociliated epithelia.

xNubp1 Is required for the apical migration/docking of basal bodies in multiciliated epidermal cells

The presence of internal ciliary axonemes and polymerized acetylated α-tubulin structures in xNubp1 high-dose morphants suggested that basal body transport may be compromised. We went on to examine the position of basal bodies in xNubp1 morphants. In controls, Centrin-YFP was tightly localized at distinct foci on the apical surface of ciliated cells and absent from deeper areas of the cell as expected (Fig. 4A). xNubp1 morphants showed a clear dose-dependent phenotype in terms of basal body migration and docking. At high MO amounts (15–20 ng), basal bodies were almost exclusively found deep within the cell body (Fig. 4B); while at lower amounts (5–8 ng) the majority reached the apical surface. At intermediate amounts of MO (8–13 ng), basal bodies were seen both at the apical surface in addition to deep within the cell, with considerable variation from cell to cell within each tadpole (Fig. 4C). Even morphant cells, in which the basal bodies migrated to the apical surface, had polymerized acetylated α-tubulin structures just below the apical surface and displayed incorrect basal body spacing (Fig. 4E). To confirm these results, we examined ciliated cells using TEM. Basal bodies in xNubp1 morphants failed to localize and dock to the apical surface of ciliated cells (Fig. 4G), which is consistent with live fluorescent imaging and immunostaining data. Immunostaining with Zo-1 (Supplementary Fig. 2H) and e-cad (data not shown) confirmed that apico-basal polarity was not affected in morphant embryos. Taken together, these data suggest that the defect in ciliogenesis observed in xNubp1 high-dose morphants is due to a failure of basal body migration and docking at the apical surface.

xNubp1 is required for polarized ciliary beating and basal body polarization

In order for ciliated cells across ciliated epithelia to undergo polarized beating, the basal bodies must first be polarized correctly (Mitchell et al., 2007; Park et al., 2008). In low-dose xNubp1 morphants, the majority of the ciliated cells projected cilia which appeared normal (data not shown). However, as mentioned above, even those embryos failed to undergo the characteristic drifting motion caused by the polarized beating of the epidermal ciliated cells, suggesting that polarized ciliary beating and directional flow was disrupted. In order to examine the directional fluid flow we used quantum dot (QD) nanocrystals in combination with live imaging. We observed distinct directional (anterior to posterior) fluid flow across the epidermis of control embryos (Fig. 5A; Supplementary Movie 1); however, xNubp1 low-dose morphants showed impaired directional fluid flow across the epithelium (Fig. 5B; Supplementary Movie2). The presence of cilia on the epidermis of these embryos was subsequently confirmed by immunostaining with acetylated α-tubulin (data not shown). Co-injection of xNubp1 mRNAwith the MO partially rescued this phenotype (Fig. 5C). In order to assess whether the motility of cilia was affected in morphant embryos, we used live bright field imaging. Ciliary beating in xNubp1 morphants was disorganized and cilia did not beat in a synchronized whip-like manner (Supplementary Movies 3 and 4). Instead, their beating was asynchronous and individual cilia moved slowly and appeared to be more rigid than in controls (Supplementary Movie 5).

Supplementary material related to this article can be found online at http://dx.doi.org/10.1016/j.ydbio.2013.05.004.

Following basal body docking during ciliogenesis, basal bodies must be polarized along the long axis (A–P) of the embryo in order to create directional fluid flow (Mitchell et al., 2007,2009; Park et al., 2008; Werner et al., 2011). Since xNubp1 knockdown led to decreased fluid flow and disorganized ciliary beating, we sought to determine whether xNubp1 was also necessary for the polarization of basal bodies. To assess the planar polarization of basal bodies, embryos were co-injected with Centrin-RFP to mark the basal body and Clamp-GFP to mark the striated rootlet (Mitchell et al., 2007,2009; Park et al., 2008; Werner et al., 2011). From these experiments, it became clear that in xNubp1 morphants with apically localized basal bodies, spacing and polarity were both compromised. Confocal imaging and quantification of the polarity using circular plots of the angular orientation and the circular standard deviation (CSD) showed that knockdown of xNubp1 led to a great deal of variation with regards to angular orientation of basal bodies (Fig. 5E and G), compared to that of control embryos (Fig. 5D and F). In addition, as noted above, the spacing between the basal bodies on these cells was also compromised (Fig. 5E). The CSD of xNubp1 morphants (Fig. 5G) was considerably higher (39.4°) than that of controls (13.5°) (Fig. 5F). In many of the morphant ciliated cells, the angle of the rootlet seemed to be perpendicular to that of the basal body, making it difficult to quantify the polarity of those particular basal bodies (Fig. 5E′; white box). These data indicate that at low amounts of Nubp1 MO, although basal bodies reach the apical surface, they fail to space and polarize correctly.

Loss of xNubp1 leads to apical actin and microtubule disorganization

The apical microtubule network in multi-ciliated cells has been shown to be essential for the correct polarization of basal bodies (Werner et al., 2011). Cytoplasmic microtubules form an organized network at the apical surface of multiciliated cells (Werner et al., 2011). These microtubules interact with basal bodies specifically at the basal foot (Gordon, 1982; Sandoz et al., 1988), and although they do not appear to be involved in the migration of basal bodies to the apical surface (Boisvieux-Ulrich et al., 1989), they are required for local coordination of basal body polarization (Werner et al., 2011). In order to visualize the apical network of microtubules, a GFP-tagged enconosin binding domain (EMTB-3XGFP) construct was used. Embryos injected with EMTB-3XGFP and Centrin-RFP displayed an organized interconnected apical network of microtubules and basal bodies (Supplementary Fig. 4A and C). In xNubp1 morphants, this apical network was disorganized (Supplementary Fig. 4B and D) and in cells with internal basal bodies the microtubule network formed around the internal basal bodies (Supplementary Fig. 4B, last panel). However, the apical microtubule network appeared much more organized in low-dose morphant ciliated cells (data not shown). These data show that the apical microtubule network in xNubp1 morphant ciliated cells is compromised, and may partly cause the basal body rotational polarity defects seen in xNubp1 morphants. However, the microtubules were still able to organize around basal bodies and therefore the unorganized microtubule network at the apical surface may be a consequence of the basal body spacing problems and the reduced number of basal bodies properly docked at the apical surface in xNubp1 intermediate-dose morphants.

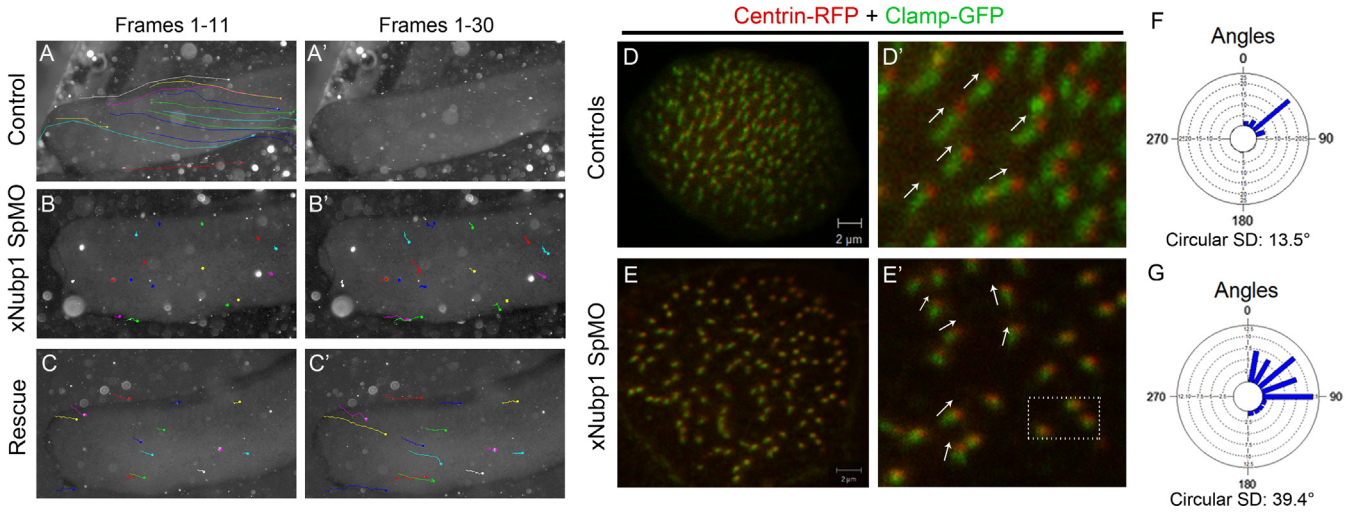

Fig. 5. xNubp1 knockdown disrupts directional fluid flow and basal body polarization. ((A)–(C)) The flow of QDs was tracked along the surface of the embryos from anterior to posterior. (A) In control embryos, QDs flow rapidly from dorso-anterior to ventral-posterior. (B) xNubp1 morphants (7 ng) show severely disrupted fluid flow. (C) Co-injection of xNubp1 MO with xNubp1 mRNA (114 pg) partially rescues ciliary flow. ((D) and (E)) Confocal images of Centrin2-RFP and Clamp-GFP. (D) Basal bodies in controls are polarized along the anterior–posterior axis in the direction of the effective stroke (Direction of polarity is depicted by white arrows). (E) Knockdown of xNubp1 (6 ng) leads to a great deal of variation with regards to angular orientation of basal bodies. Many of the morphant ciliated cells the angle of the rootlet is perpendicular to that of the basal body (white box), making it difficult to quantify the polarity of the basal bodies. ((F) and (G)) Quantification of the polarity using circular plots of the angular orientation and the Circular Standard Deviation (CSD). The blue bars depict the mean direction of the cilia and the bar length depicts the variance around the mean. CSD of controls (F) is considerably lower than that of xNubp1 low-dose morphants (G).

The apical surface of *X. laevis* ciliated epidermal cells have a dense meshwork of actin (Nishikawa et al., 1992; Park et al., 2006) comprised of two distinct but interconnected pools; the apical and sub-apical pool of actin (Werner et al., 2011). Loss of apical and sub-apical actin localization leads problems with basal body localization and polarity, respectively (Boisvieux-Ulrich et al., 1990; Park et al., 2006,2008; Werner et al., 2011). The PCP pathway effector RhoA regulates actin organization (Hall, 1998), and recent work has shown that RhoA is enriched at the apical surface of ciliated cells (Pan et al., 2007; Park et al., 2008), and is essential for the apical docking of basal bodies by mediating apical actin enrichment (Pan et al., 2007). Examination of the localization of RhoA and Dvl; another PCP pathway member which associates with and activates Rho (Habas et al., 2001; Park et al., 2008) and is required for basal body docking and planar polarization of basal bodies (Park et al., 2008), in high-dose morphants revealed that these proteins were mislocalized. Dvl, total RhoA and active RhoA localized with the cell body together with internal basal bodies (Supplementary Fig. 5). Since RhoA has a critical role in the formation of the apical actin network, we therefore wanted to first examine if apical actin was affected in xNubp1 high-dose morphants with internalized basal bodies. Fluorescent immunostaining revealed that xNubp1 high-dose morphant embryos failed to accumulate the dense actin meshwork (Supplementary Fig. 6B) found in control (Supplementary Fig. 6A) and CoMO (data not shown) injected ciliated cells, but retained the cortical actin at cell borders (Supplementary Fig. 6B and D). These data indicate that the failure of basal body apical migration in high-dose morphants leads to a mislocalization of PCP pathway members and as a result, apical actin fails to accumulate.

We next wanted to examine the apical and sub-apical actin networks in xNubp1 low-dose morphants. As shown in Fig. 6B and D, apical actin, although enriched, appeared reduced and less organized in xNubp1 low-dose morphants which had apically localized basal bodies and extended cilia outward (Fig. 6B). Specifically, the apical actin in morphants failed to organize into an interconnected network but rather appeared as disconnected puncta. Co-injection of xNubp1 mRNA partially rescued the apical actin disorganization (Supplementary Fig. 4E and F). The sub-apical actin pool has been shown to be important for both the spacing of basal bodies as well as overall rotational polarity at a distance. Use of Cytochalasin D to disrupt the sub-apical actin connections between basal bodies, leads to both loss of spacing as well as loss of cell-wide rotational polarity and metachronal synchrony (Werner et al., 2011), raising the possibility that loss of xNubp1 may also disrupt this network. We observed that the sub-apical actin network in xNubp1 low-dose morphants was nearly absent (Fig. 6D″). We therefore went on to examine RhoA localization in low-dose morphant embryos and saw that despite the loss of sub-apical actin and disorganized apical actin; RhoA was in fact apically enriched in these cells (Fig. 6E). Using an active RhoA sensor (rGBD-GFP) we examined whether RhoA was active in xNubp1 low-dose morphant ciliated cells. As shown in Fig. 6F, we saw that this was in fact the case. These data suggest that loss of Nubp1 may be affecting the formation/stabilization of the apical and sub-apical actin networks through a Rho/PCP independent mechanism.

The effect of xNubp1 down regulation on the apical and sub-apical actin cytoskeleton of ciliated cells prompted us to examine xNubp1 localization in these cells. Using a GFP tagged variant of Nubp1, we saw that xNubp1 was apically enriched and co-localized with the apical actin cytoskeleton in ciliated cells (Supplementary Fig. 6E–G) while no co-localization could be detected on the cortical actin cytoskeleton (data not shown). Interestingly, we also saw that GFP-Nubp1 was localized on the mitotic spindle of non-ciliated cells of the epidermis undergoing cell division (Supplementary Fig. 6H–K and Movie 6). To validate these findings, both flag tagged and HA tagged versions of Nubp1 were also generated, and both gave similar results in embryos co-stained with phalloidin, showing a clear apical enrichment of xNubp1 and co-localization with the apical actin network (data not shown). We went on to examine the possibility of direct binding of Nubp1 on actin and carried out co-immunoprecipitation using tagged versions of xNubp1. However,

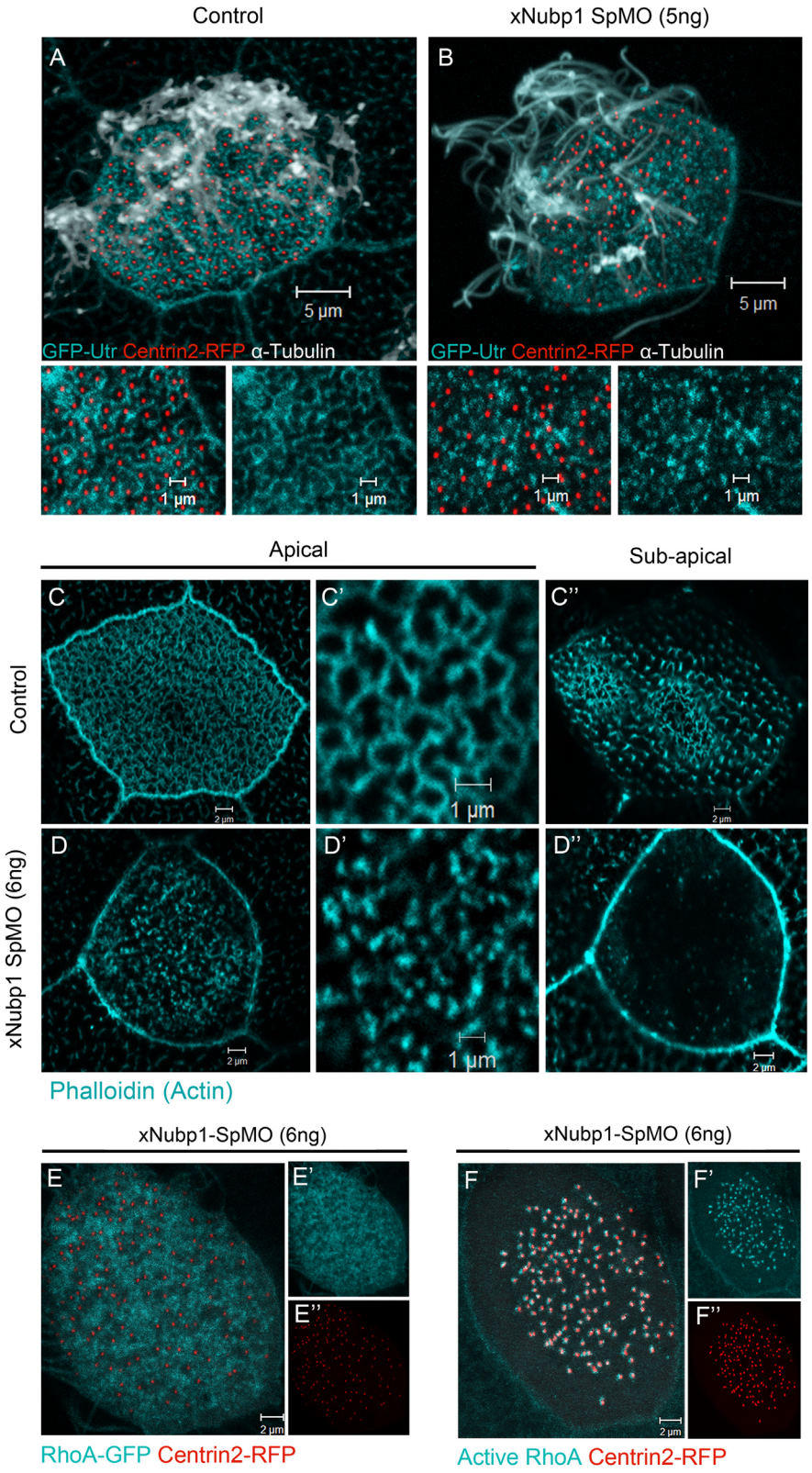

Fig. 6. xNubp1 is required for apical actin organization but does not act through RhoA. (A) Apical actin (GFP-Utrophin) forms an organized enriched meshwork around docked basal bodies (Centrin2-RFP) in control multi-ciliated cells. Cilia project from the apical surface. (B) Basal bodies in low-dose xnubp1 morphants have migrated and docked to the apical surface and extended cilia. However, the apical actin network remains punctate (C, C′) Control ciliated cell has an organized apical actin network. (C″) Roughly 0.4 μm below the apical surface the distinct sub-apical pool of actin is present. ((D), (D′)) The apical actin in xNubp1 low-dose morphant multi-ciliated cells is not as enriched as in controls and appears punctate. (D″) Sub-apical actin is almost entirely absent. (E) xNubp1low dose morphants have apically enriched RhoA-GFP and the basal bodies have reached the apical surface (E′). (F) RhoA is active at the apical surface of low-dose morphant ciliated cells with apical basal bodies (F″).

no association between actin and xNubp1 was detected (data not shown), suggesting that xNubp1 may be interacting with actin indirectly or interacting specifically with F-actin.

Supplementary material related to this article can be found online at http://dx.doi.org/10.1016/j.ydbio.2013.05.004.

Loss of xNubp1 leads to apical actin destabilization

Despite apical enrichment of RhoA in xNubp1 low-dose morphants, the apical actin failed to organize. Therefore, it is possible that the lack of organization in morphants is stemming from an inability of the cell to stabilize this network in the absence of xNubp1. The co-localization of xNubp1 with the apical actin network in controls is consistent with such a role for xNubp1 in ciliated cells. To examine this possibility, we decided to compare the dynamics of the apical actin network in control and morphant embryos using fluorescence recovery after photobleaching (FRAP) experiments. A small region of the apical actin network was bleached in each cell and the recovery was then monitored. As shown in Fig. 7A and B and supplementary Fig. 4G, the apical actin network in control cells did not fully recover within the acquisition period. In order for control ciliated cells to fully recover, they required roughly 5 to 10 min ($t1/2 = 86$ s; data not shown), suggesting that this network is very stable with little polymerization/depolymerisation taking place after it is established. Non-ciliated neighboring cells on the other hand had a highly dynamic apical actin network, with fast recovery rates (data not shown). In low-dose xNubp1 morphants; the recovery rate of apical actin in ciliated cells was much faster ($t1/2$ of 17.4 s), showing full recovery within 1 min (Fig. 7C and D; Supplementary Fig. 4H). It should be noted that an accurate $t1/2$ was difficult to obtain as was the immobile fraction in both controls and morphants. In controls, full recovery was too long (at least 5 min and up to ten) and movement of the embryo during this period made accurate measurements very difficult. In low-dose morphants, the actin network was extremely dynamic, again making accurate measurements difficult since the network was remodelled by the time full recovery was reached.

To get a better look at actin dynamics in control and low-dose morphant cells, we also generated time-lapse sequences of adjacent ciliated and non ciliated cells. The apical actin network of control ciliated cells remained unchanged during the acquisition period, while the apical actin of the non-ciliated control cells was quite dynamic and was completely remodeled within the acquisition period (Supplementary Movie 7). However, in xNubp1 low-dose morphants, the apical actin network of the ciliated cells was

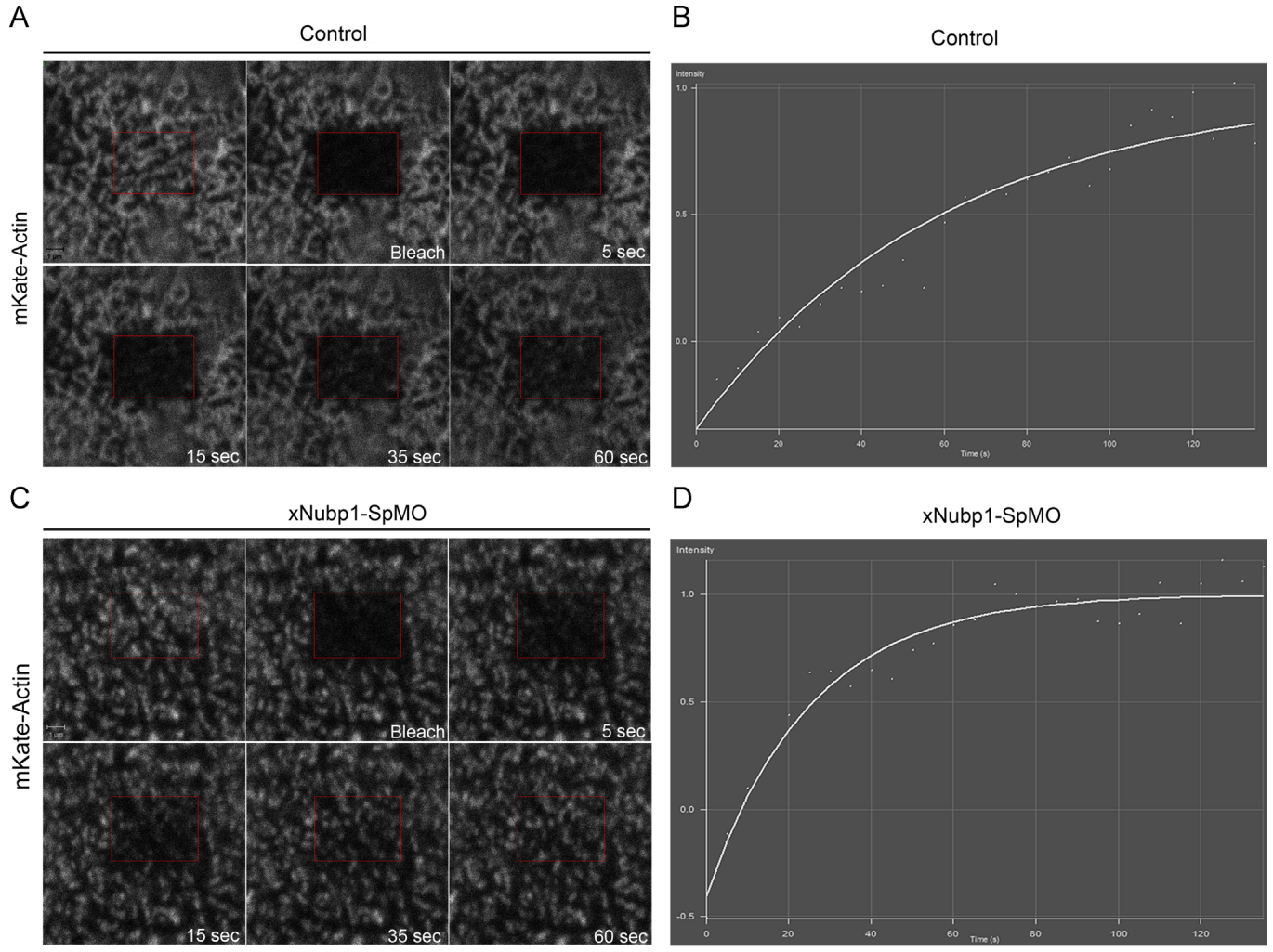

Fig. 7. Loss of xNubp1 destabilizes the apical actin network of multiciliated cells. ((A) and (B)) Fluorescence recovery after photobleaching (FRAP) experiment on a stage 29 embryo expressing mKate2-actin. (A) Bleached apical actin region of a control ciliated cell shows little recovery within 1 min. (B) Normalized graph of FRAP experiment shows that cell continues recovering after 2 min (B). ((C) and (D)) FRAP experiment on stage 29 embryo injected with xNubp1–SpMO and mKate2-actin. (C) Bleached region of morphant ciliated cell recovers fully within 1 min. (D) Normalized graph of FRAP experiment depicting signal intensity of bleached region over time. Graph shows full recovery within the acquisition window.

quite dynamic and was also completely remodeled within the time frame of the movie (Supplementary Movie 8). These results suggest that despite apical enrichment and activation of RhoA in the absence of xNubp1, ciliated cells are unable stabilize the apical actin network. The lack of a stable apical and sub-apical actin network explains both the loss of polarity and irregular spacing of basal bodies in xNubp1 morphants and suggests a role for xNubp1 in stabilizing the apical and sub-apical actin networks of multiciliated cells.

Supplementary material related to this article can be found online at http://dx.doi.org/10.1016/j.ydbio.2013.05.004.

Live imaging of actin and basal bodies during ciliated cell intercalation

The above data suggest a role for xNubp1 in the generation/maintenance of the apical and sub-apical actin networks of ciliated cells. Since basal body transport is also dependent on acto-myosin (Boisvieux-Ulrich et al., 1990; Dawe et al., 2007), these results raised the possibility that problems with basal body transport presented in xNubp1 morphants, may also be due to problems with actin organization and stability. Although the actin cytoskeleton is important for the apical migration of basal bodies, the precise mechanism through which actin is involved in this process is not clear. Therefore, in order to get a better understanding of this process, as well as to determine the temporal relationship between basal body migration and the actin cytoskeleton during ciliogenesis, we decided to image the intercalation of multiciliated epidermal cells live.

Stage 20–22 embryos expressing a GFP tagged form of the F-actin binding domain of Utrophin and Centrin2-RFP were imaged periodically during ciliated cell intercalation. Ciliated cells, which were just beginning to intercalate displayed a dense cortical actin network at their apical region (Fig. 8A). Right below the surface of the epidermis, the actin-based protrusive activity of the cortical actin at the apical "neck" region of the intercalating cell was also visible (Fig. 8B). At this stage, the basal bodies were observed deep within the cell (Fig. 8A and B last panel). From the moment the apical surface of the intercalating cell became visible, apical actin enrichment was also present (Fig. 8D′). Some basal bodies were observed at the apical surface from the onset of intercalation and as the diameter of the apical surface increased, basal bodies successively reached and docked at the apical surface. Three-dimensional reconstructions of optical sections taken during intercalation showed that once intercalation began, basal bodies started migrating towards the apical surface en masse (Fig. 8D″). Most basal bodies reached the apical region of the cell even before the cell had fully intercalated and remained there until they docked. Although apical actin was enriched very early on during intercalation, it was composed of individual puncta and did not form an organized network. In general, the apical surface of the cell at this early intercalation stage and throughout the intercalation process displayed two distinct pools of actin. The punctate apical actin described above, and the cortical actin network which resembled a "lamellar ring" (Fig. 8D′ most visible at 37 min). Once all the basal bodies reached the apical surface and the cell had fully intercalated, the apical actin matured into an organized network and the cortical actin no longer resembled a lamellar ring.

Of special interest, was the observation that within the intercalating cell, there was a network of cytoplasmic actin filaments, which surrounded the basal bodies and extended towards the cell periphery, making connections to the cell cortex (Fig. 8B last panel, F′ bottom panel). This internal actin pool surrounded the basal bodies and formed connections between them as they migrated toward the apical surface. When all the basal bodies reached the apical surface, the internal actin spread out just below the apical actin network and appeared to mature into the characteristic sub-apical actin network (Fig. 8C; data not shown). These data reveal that apical actin is enriched from the onset of intercalation and becomes organized after the cell intercalates and basal bodies dock. In addition, it is clear that actin forms another network around the internal migrating basal bodies and actin cables project from the actin-basal body cluster toward the cell cortex. This actin network appears to connect the basal bodies, keeping them clustered and at the same time anchoring them to the cell cortex.

In light of these new observations regarding actin cytoskeleton and basal body migration during ciliogenesis, we decided to examine basal body migration and actin organization in xNubp1low-dose morphants during intercalation. Like controls, xNubp1 morphants showed early apical actin enrichment with punctate F-actin foci appearing at the apical region of newly intercalating ciliated cells as well as a lamellar ring at the cell periphery (Fig. 8E and F″). In fact, the apical actin between control and morphant cells was indistinguishable at this stage. However, the actin network surrounding the migrating basal bodies within the cytoplasm was substantially reduced with few actin cables reaching the cortex in xNubp1 morphants (Fig. 8F″), suggesting that the basal body migration defect in morphants may be due to defects in the internal actin network. When the cells had fully intercalated, differences between the apical actin of controls and morphants also became visible, with the controls displaying mature network of apical actin (Fig. 8G′), while in morphants this failed to organize and remained as punctate F-actin foci (Fig. 8G″). We also observed that when pushed using a coverslip, the apical membrane of control ciliated cells would deform, caving in at places and rarely would the entire cell surface be parallel to the coverslip, presumably due to the apical actin networks stiffness and resistance to the deforming force. However, in morphants the pressure would cause the apical membrane to become flat all along the coverslip (data not shown), suggesting loss of stiffness and ability to resist deformation. Collectively, these findings suggest that defects in basal body transport, docking and polarity in xNubp1 morphants are likely due to defects in the actin cytoskeleton and provide new insights regarding the mechanism of basal body transport and the involvement of the actin cytoskeleton in ciliogenesis.

Discussion

In this study we show that xNubp1 is expressed throughout early development; displaying elevated expression in neural tissues, localization at the mitotic spindle during cell division and to the apical actin network in multiciliated epidermal cells. Using three distinct morpholino oligonucleotides, which block either translation or splicing, we found that complete loss of xNubp1 is lethal, in agreement with a generalized role of Nubp1 for cell survival. However, at lower amounts of MO, embryos develop to tadpole stages, however, display defects suggestive of problems with convergent extension movements. We go on to show that xNubp1 is in fact required for convergent extension and neural tube closure. Surprisingly, we also found that xNubp1 is required for ciliogenesis in multiciliated epidermal cells and in GRP mono-ciliated cells. Specifically, xNubp1 appears to be important in two processes required for ciliogenesis, basal body transport to the apical surface and regulation of the actin networks which are necessary for basal body migration and docking. Finally, live confocal imaging of the actin cytoskeleton and basal bodies in intercalating multiciliated cells has allowed us to observe the formation of the apical actin network and also to image an internal pool of actin which surrounds the migrating basal bodies. By

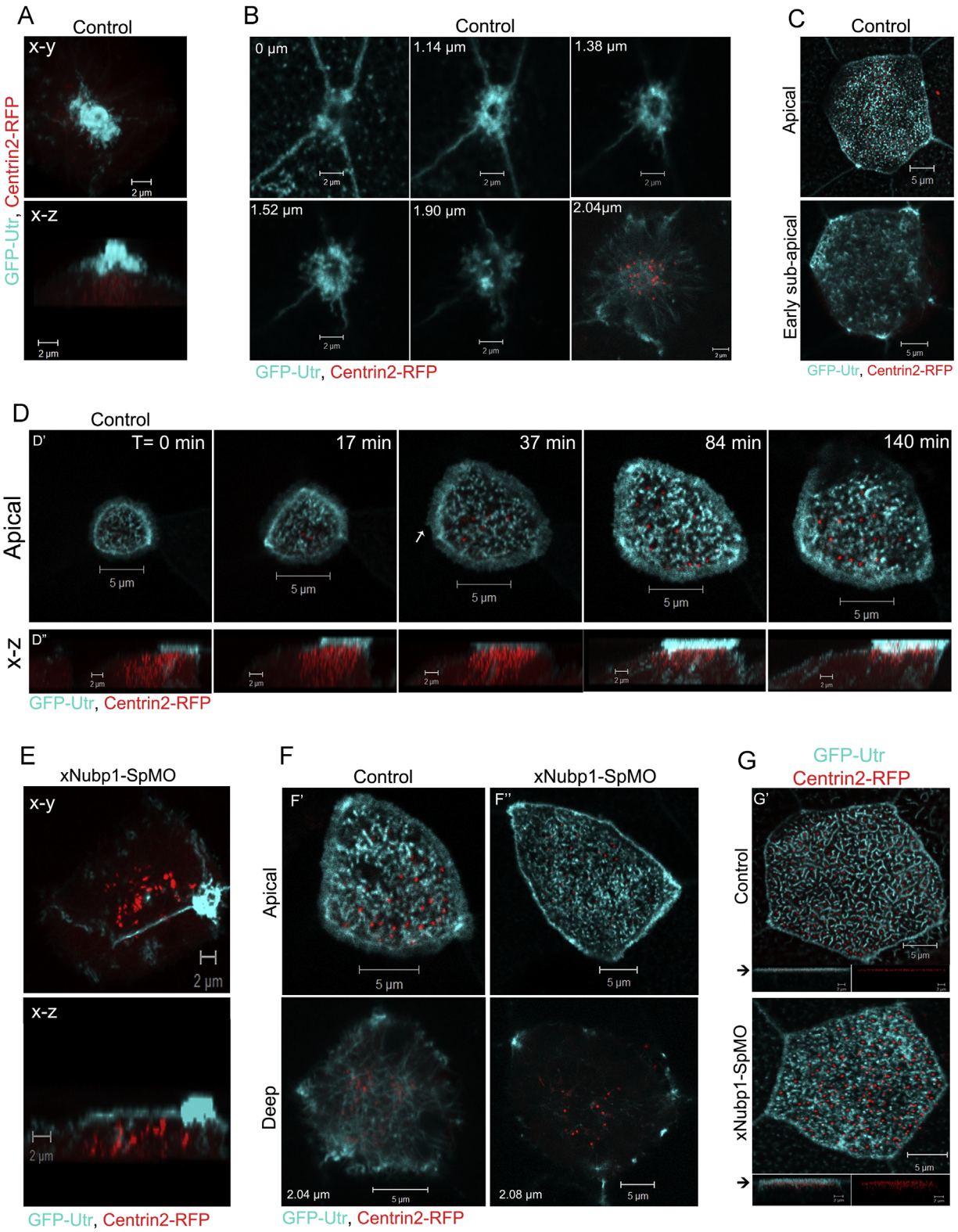

Fig. 8. Actin Cytoskeleton during ciliated cell intercalation and basal body migration. Live confocal imaging of stage 20–30 control and morphant embryos expressing GFP-Utr and Centrin2-RFP. (A) *x–y* and *x–z* projections of a stage 20 ciliated cell beginning the intercalation process, showing enrichment of F-actin at the apical region of the cell and internal basal bodies. (B) Optical z-sections of a newly intercalating ciliated cell. Cortical actin based protrusions are visible at the apical region of the intercalating cells. Within the cell body (2.04 μm), an internal actin network surrounds the migrating basal bodies and extends toward the cell cortex. (C) Fully intercalated ciliated cell of a stage 23 embryo. The apical actin pool is still punctate and has not yet organized into a network. The lamellar ring-like cortical actin structure is no longer present. The sub-apical actin network is just beginning to form. (D′) Time points of a stage 21–22 embryo showing the apical surface of an intercalating ciliated cell. The enriched apical actin pool is present from the beginning of intercalation ($T=0$ min). As the cell intercalates, basal bodies sequentially dock at the apical surface. During intercalation we also observe a "lamellar ring" at the apical cortex of the intercalating cell (arrow in $T=37$ min). (D″) 3D reconstruction of intercalating cell showing the basal bodies are slowly migrating towards the apical surface. Even before the cell has fully intercalated, most of the basal bodies have reached the apical surface. (E) *x–y* and *x–z* projections of a ciliated cell of a stage 20 xNubp1 low-dose morphant embryo beginning the intercalation process. (F) Intercalating control (F′) and xNubp1morphant (F″) ciliated cell. Deep sections show that the internal actin pool in morphants is severely reduced compared to controls. (G) Fully intercalated control (G′) and xNubp1low-dose morphant cell (G″) of stage 29–30 embryos. The apical actin pool in control ciliated cell has formed an organized network whereas the apical actin pool of the morphant ciliated cell remains unorganized and punctate. Bottom panels show *x–z* projections depicting apically localized basal bodies. Black arrows indicate apical surface.

depleting xNubp1, we have shown that the internal actin network is indeed essential for basal body migration.

Although the overall phenotype of xNubp1 knockdown would appear to be related to disruption of PCP signaling, we show that this is not the case. In addition to the long established role of PCP in polarized cell movements like convergent extension (Heisenberg et al., 2000; Sokol, 1996; Tada and Smith, 2000; Wallingford et al., 2000, 2002; Wallingford and Harland, 2002; Ybot-Gonzalez et al., 2007), there is now mounting evidence that PCP proteins are important for ciliogenesis (Park et al., 2006, 2008; Wallingford and Mitchell, 2011). Core members of the PCP pathway like Dvl, have been clearly linked to both processes (Park et al., 2006, 2008; Tada and Smith, 2000; Wallingford, 2006, 2010; Wallingford and Mitchell, 2011). Dvl's role in cell polarity during convergent extension is well documented (Wallingford and Habas, 2005; Wallingford and Harland, 2001, 2002; Wallingford et al., 2000), as is the Dvl-mediated activation of Rho (Habas et al., 2001; Park et al., 2008; Schlessinger et al., 2009). In Xenopus multiciliated cells, it has been shown that Dvl is essential for ciliogenesis and that it is required for Rho activation at the apical surface (Park et al., 2008). However, unlike Inturned morphants, where apical enrichment of RhoA is lost (Park et al., 2006) in multiciliated cells, RhoA localization is unaffected in Dvl morphants (Park et al., 2008). In both cases though, effects on RhoA activation or localization at the apical membrane result in loss of the apical actin network (Park et al., 2006, 2008). Interestingly, although the localization of such PCP members is affected in xNubp1 high-dose morphants due to basal body migration failure, in low-dose morphants, basal body migration to the apical surface is unaffected and just like Dvl knockdown, RhoA apical enrichments is not affected. Unlike Dvl morphants however, xNubp1 low-dose morphants show normal RhoA activation and in fact, they display enriched apical actin compared to non-ciliated cells, further supporting the conclusion that neither RhoA localization nor its activation are affected by the loss of xNubp1. Even in the presence of apically localized active RhoA, basal body docking is still perturbed, basal body spacing becomes irregular, and drastic effects on the motility and synchronization of morphant cilia are observed in xNubp1 low-dose morphants. In part, the phenotype may arise from rotational polarity issues but these are relatively mild. Unlike Dvl, which leads to randomization in terms of rotational polarity, in xNubp1 morphants rotational polarity is only affected at a distance since adjacent basal bodies maintain similar orientation. Overall, these data suggest that Nubp1 is not acting through Dvl and that despite their similarities, the phenotypes are quite distinct.

A possible explanation of the xNubp1 phenotype emerged when we noted that despite the fact that the apical actin of low-dose morphant ciliated cells was enriched, it appeared disorganized and failed to form an interconnected network. Time lapse sequences as well as FRAP experiments show that the apical actin network of control ciliated cells is extremely stable, with little remodeling taking place once it is set and basal bodies have docked. However, in xNubp1 morphants this network is highly dynamic, being remodeled within a very short time. This suggests that xNubp1 may have a role in stabilizing the apical actin network in ciliated cells, and this is supported further by the finding that xNubp1 co-localizes with the apical actin cytoskeleton in these cells. However, the exact mechanism through which xNubp1 may be eliciting this effect remains to be elucidated.

Our results point to an additional role of xNubp1 in the transport of basal bodies rather than their maintenance at the apical surface. In high-dose morphants, we observed that nearly all the basal bodies remain deep within the cytoplasm where they form. There, they are associated with Dvl and active Rho and even form internal ciliary axonemes. This shows that apical docking is not required for cilia assembly, which is in agreement with data concerning the Dvl, Celsr2 and Celsr2+3 mutants (Park et al., 2008; Tissir et al., 2010). The presence of active RhoA around these internal basal bodies once again shows that xNubp1 does not act through RhoA, and that the defect in basal body transport is consistent with a role of xNubp1 in the regulation of actin dynamics in relation to ciliogenesis. xNubp1 is also involved in ciliogenesis in motile mono-ciliated GRP cells. On the GRP, a single short cilium forms at the center of each cell and subsequently localizes to the posterior of the cell and lengthens in the process. These polarized GRP cilia beat in a circular motion to produce leftward that is important for left–right asymmetry (Blum et al., 2009; Schweickert et al., 2007). PCP has also been linked to the posterior localization of these GRP cilia and for the establishment of L–R asymmetry (Antic et al., 2010). However, the mechanical process of cilia posteriorization is not completely understood. xNubp1 knockdown leads to a 2.8 fold decrease in cilia length. Some cilia also appear to be more centrally localized. These GRP cilia defects observed consequently lead to a disruption of L–R patterning, which is most likely caused by a decrease or loss of flow across the GRP. In light of the effect of xNubp1 knockdown on apical actin, the lack of polarization and reduced length of the cilia may be due to a mechanical perturbation of basal body posteriorization, since the basal body docks and extends a cilium outward in xNubp1 morphant GRP cells.

During the past decade, a great deal of research has focused on uncovering the mechanisms of ciliogenesis. The mechanical basis of basal body apical migration in multi-ciliated cells and the importance of the actin cytoskeleton in this process however, have not yet been examined thoroughly. A study using the drug Cytochalasin D to perturb the actin cytoskeleton revealed that the migration and docking of basal bodies rely on an intact actin cytoskeleton (Boisvieux-Ulrich et al., 1990). In Xenopus however, it is difficult to examine the role of the actin cytoskeleton in basal body migration using drugs which target the actin cytoskeleton due to the fact that basal body migration is concomitant with cell intercalation, and therefore disrupting the actin cytoskeleton will lead to a failure of ciliated cells to intercalate.

Our data lead to several new key observations regarding the formation and importance of the actin cytoskeleton in multi-ciliated cells. We show that the apical actin network, which is a key structural component of multi-ciliated cells, initially manifests as punctate apical actin enrichment at the onset of cell intercalation, and is later organized into an interconnected network. In addition, we show that there is an internal actin network surrounding the migrating basal bodies and making connections between them. We observed that this internal actin network was still present just below the apical actin when basal bodies reached the surface. When the basal bodies dock and apical actin matures into a network, the internal actin network is replaced by the sub-apical actin pool. Although we did not directly observe this transition, it is likely that the internal actin network is remodeled into the sub-apical actin network. So it appears that both the apical and the internal actin networks found in ciliated cells are formed independently and are present at the onset of ciliated cell intercalation. In xNubp1 morphants at early stages of intercalation, the internal actin pool surrounding the basal bodies appears very weak and lacks organization compared to controls. The apical actin however is enriched early on and is comparable to controls, but fails to mature into a network later on. The failure of basal bodies to migrate in high-dose cells suggests that loss of xNubp1 at this stage has a preferential effect on the deep actin network without which basal body migration fails.

If xNubp1 down regulation does not affect cell polarity directly and is not involved in the PCP pathway, then how can defects in convergent extension movements be explained? During convergent

extension, cells mediolaterally intercalate (Wallingford et al., 2002) in order to help close the neural tube and elongate the vertebrate body A–P axis (Wallingford and Harland, 2002). Acto-myosin in cells and tissues has a number of roles and is the driving force behind coordinated cell movements like convergent extension (Kim and Davidson, 2011; Rauzi and Lenne, 2011; Skoglund et al., 2008). In fact, brief exposure to actin destabilizing agents like latrunculin B during Xenopus gastrulation; despite a transient effect on actin stability, leads to long term defects that are strikingly similar to those described by inhibition of the PCP pathway, including shortened anterior posterior axis and curved backs (Kim and Davidson, 2011; Zhou et al., 2009). It is possible that loss of xNubp1 leads to a similar destabilization of the acto-myosin cytoskeleton in that context, thus producing a PCP-like phenotype. It is also possible that xNubp1 is a member of a parallel pathway, which regulates the actin cytoskeleton, or is possibly a downstream effector of the PCP pathway. It would be interesting to examine the effects of xNubp1 down regulation on the cytoskeleton, protrusive activity and cell polarity in mesodermal and neural tissues undergoing convergent extension, in order to better understand the mechanism through which loss of xNubp1 inhibits mediolateral intercalation. Overall, this study identifies novel roles for xNubp1 in ciliogenesis and convergent extension movements both of which appear to stem from the regulation of actin dynamics by xNubp1. The mechanism through which xNubp1 regulates the actin cytoskeleton as well as the precise way xNubp1 is involved in convergence extension movements will be the focus of future studies.

Acknowledgements

We would like to thank Drs. John Wallingford, Brian Mitchell, Chenbei Chang, Reinhard Köster and Martin Blum for kindly providing plasmids. We would like to thank Dr. Kyriacos Kyriacou and Marianna Nearchou at Cyprus Institute of Neurology and Genetics for their help with electron microscopy and allowing us to use their facility. We also thank Katerina Othonos and the members of the Skourides lab for their help. Funding was provided by the Cyprus Research Promotion Foundation (PENEK/0609/51) and co-funded by the Structural Funds of the European Union.

Appendix A. Supporting information

Supplementary data associated with this article can be found in the online version at http://dx.doi.org/10.1016/j.ydbio.2013.05.004.

References

Antic, D., Stubbs, J.L., Suyama, K., Kintner, C., Scott, M.P., Axelrod, J.D., 2010. Planar cell polarity enables posterior localization of nodal cilia and left–right axis determination during mouse and Xenopus embryogenesis. PLoS One 5, e8999.
Baker, K., Beales, P.L., 2009. Making sense of cilia in disease: the human ciliopathies. Am. J. Med. Genet. C Semin. Med. Genet. 151C, 281–295.
Blum, M., Beyer, T., Weber, T., Vick, P., Andre, P., Bitzer, E., Schweickert, A., 2009. Xenopus, an ideal model system to study vertebrate left–right asymmetry. Dev. Dyn. 238, 1215–1225.
Boisvieux-Ulrich, E., Laine, M.C., Sandoz, D., 1985. The orientation of ciliary basal bodies in quail oviduct is related to the ciliary beating cycle commencement. Biol. Cell 55, 147–150.
Boisvieux-Ulrich, E., Laine, M.C., Sandoz, D., 1989. In vitro effects of colchicine and nocodazole on ciliogenesis in quail oviduct. Biol. Cell 67, 67–79.
Boisvieux-Ulrich, E., Laine, M.C., Sandoz, D., 1990. Cytochalasin D inhibits basal body migration and ciliary elongation in quail oviduct epithelium. Cell Tissue Res. 259, 443–454.
Boisvieux-Ulrich, E., Sandoz, D., Allart, J.-P., 1991. Determination of ciliary polarity precedes differentiation in the epithelial cells of quail oviduct. Biol. Cell 72, 3–14.
Bowes, J.B., Snyder, K.A., Segerdell, E., Jarabek, C.J., Azam, K., Zorn, A.M., Vize, P.D., 2010. Xenbase: gene expression and improved integration. Nucleic Acids Res. 38, D607–612.
Christodoulou, A., Lederer, C.W., Surrey, T., Vernos, I., Santama, N., 2006. Motor protein KIFC5A interacts with Nubp1 and Nubp2, and is implicated in the regulation of centrosome duplication. J. Cell Sci. 119, 2035–2047.
Chung, M.-I., Peyrot, S.M., LeBoeuf, S., Park, T.J., McGary, K.L., Marcotte, E.M., Wallingford, J.B., 2012. RFX2 is broadly required for ciliogenesis during vertebrate development. Dev. Biol. 363, 155–165.
Dawe, H.R., Farr, H., Gull, K., 2007. Centriole/basal body morphogenesis and migration during ciliogenesis in animal cells. J. Cell Sci. 120, 7–15.
Frisch, D., Farbman, A.I., 1968a. Development of order during ciliogenesis. Anat. Rec. 162, 221–231.
Frisch, D., Farbman, A.I., 1968b. Development of order during ciliogenesis. Anat. Rec. 162, 221–232.
Goetz, S.C., Anderson, K.V., 2010. The primary cilium: a signalling centre during vertebrate development. Nat. Rev. Genet. 11, 331–344.
Gomperts, B.N., Gong-Cooper, X., Hackett, B.P., 2004. Foxj1 regulates basal body anchoring to the cytoskeleton of ciliated pulmonary epithelial cells. J. Cell Sci. 117, 1329–1337.
Gordon, R.E., 1982. Three-dimensional organization of microtubules and microfilaments of the basal body apparatus of ciliated respiratory epithelium. Cell Motil. 2, 385–391.
Habas, R., Kato, Y., He, X., 2001. Wnt/frizzled activation of Rho regulates vertebrate gastrulation and requires a novel formin homology protein Daam1. Cell 107, 843–854.
Hall, A., 1998. Rho GTPases and the actin cytoskeleton. Science 279, 509–514.
Hausmann, A., Aguilar Netz, D.J., Balk, J., Pierik, A.J., Muhlenhoff, U., Lill, R., 2005. The eukaryotic P loop NTPase Nbp35: an essential component of the cytosolic and nuclear iron-sulfur protein assembly machinery. Proc. Nat. Acad. Sci.U.S.A. 102, 3266–3271.
Heisenberg, C.P., Tada, M., Rauch, G.J., Saude, L., Concha, M.L., Geisler, R., Stemple, D. L., Smith, J.C., Wilson, S.W., 2000. Silberblick/Wnt11 mediates convergent extension movements during zebrafish gastrulation. Nature 405, 76–81.
Hildebrandt, F., Benzing, T., Katsanis, N., 2011. Ciliopathies. N. Engl. J. Med. 364, 1533–1543.
Huang, T., You, Y., Spoor, M.S., Richer, E.J., Kudva, V.V., Paige, R.C., Seiler, M.P., Liebler, J.M., Zabner, J., Plopper, C.G., Brody, S.L., 2003. Foxj1 is required for apical localization of ezrin in airway epithelial cells. J. Cell Sci. 116, 4935–4945.
Kim, H.Y., Davidson, L.A., 2011. Punctuated actin contractions during convergent extension and their permissive regulation by the non-canonical Wnt-signaling pathway. J. Cell Sci. 124, 635–646.
Klotz, C., Bordes, N., Laine, M.C., Sandoz, D., Bornens, M., 1986. Myosin at the apical pole of ciliated epithelial cells as revealed by a monoclonal antibody. J. Cell Biol. 103, 613–619.
Koonin, E.V., 1993. A superfamily of ATPases with diverse functions containing either classical or deviant ATP-binding motif. J. Mol. Biol. 229, 1165–1174.
Leipe, D.D., Wolf, Y.I., Koonin, E.V., Aravind, L., 2002. Classification and evolution of P-loop GTPases and related ATPases. J. Mol. Biol. 317, 41–72.
Lemullois, M., Klotz, C., Sandoz, D., 1987. Immunocytochemical localization of myosin during ciliogenesis of quail oviduct. Eur. J. Cell Biol. 43, 429–437.
Lutkenhaus, J., Sundaramoorthy, M., 2003. MinD and role of the deviant Walker A motif, dimerization and membrane binding in oscillation. Mol. Microbiol. 48, 295–303.
Mitchell, B., Jacobs, R., Li, J., Chien, S., Kintner, C., 2007. A positive feedback mechanism governs the polarity and motion of motile cilia. Nature 447, 97–101.
Mitchell, B., Stubbs, J.L., Huisman, F., Taborek, P., Yu, C., Kintner, C., 2009. The PCP pathway instructs the planar orientation of ciliated cells in the *Xenopus* larval skin. Curr. Biol. 19, 924–929.
Nakashima, H., Grahovac, M.J., Mazzarella, R., Fujiwara, H., Kitchen, J.R., Threat, T.A., Ko, M.S.H., 1999. Two novel mouse genes – Nubp2, mapped to the t-complex on chromosome 17, and Nubp1, mapped to chromosome 16 – establish a new gene family of nucleotide-binding proteins in eukaryotes. Genomics 60, 152–160.
Netz, D.J.A., Pierik, A.J., Stumpfig, M., Muhlenhoff, U., Lill, R., 2007. The Cfd1–Nbp35 complex acts as a scaffold for iron–sulfur protein assembly in the yeast cytosol. Nat. Chem. Biol. 3, 278–286.
Nieuwkoop, P.D.A.F., J., 1994. Normal Table of *Xenopus laevis* (Daudin), first ed0. Garland, New York.
Nishikawa, S., Hirata, J., Sasaki, F., 1992. Fate of ciliated epidermal cells during early development of <i>Xenopus laevis</i> using whole-mount immunostaining with an antibody against chondroitin 6-sulfate proteoglycan and anti-tubulin: transdifferentiation or metaplasia of amphibian epidermis. Histochem. Cell Biol. 98, 355–358.
Pan, J., You, Y., Huang, T., Brody, S.L., 2007. RhoA-mediated apical actin enrichment is required for ciliogenesis and promoted by Foxj1. J. Cell Sci. 120, 1868–1876.
Park, T.J., Haigo, S.L., Wallingford, J.B., 2006. Ciliogenesis defects in embryos lacking inturned or fuzzy function are associated with failure of planar cell polarity and Hedgehog signaling. Nat. Genet. 38, 303–311.
Park, T.J., Mitchell, B.J., Abitua, P.B., Kintner, C., Wallingford, J.B., 2008. Dishevelled controls apical docking and planar polarization of basal bodies in ciliated epithelial cells. Nat. Genet. 40, 871–879.
Pazour, G.J., Agrin, N., Leszyk, J., Witman, G.B., 2005. Proteomic analysis of a eukaryotic cilium. J. Cell Biol. 170, 103–113.
Pazour, G.J., Witman, G.B., 2003. The vertebrate primary cilium is a sensory organelle. Curr. Opin. Cell Biol. 15, 105–110.

Pedersen, L.B., Veland, I.R., Schroder, J.M., Christensen, S.T., 2008. Assembly of primary cilia. Dev. Dyn. 237, 1993–2006.
Rauzi, M., Lenne, P.F., 2011. Cortical forces in cell shape changes and tissue morphogenesis. Curr. Top. Dev. Biol. 95, 93–144.
Roy, S., 2009. The motile cilium in development and disease: emerging new insights. Bioessays 31, 694–699.
Sandoz, D., Chailley, B., Boisvieux-Ulrich, E., Lemullois, M., Laine, M.C., Bautista-Harris, G., 1988. Organization and functions of cytoskeleton in metazoan ciliated cells. Biol. Cell 63, 183–193.
Schlessinger, K., Hall, A., Tolwinski, N., 2009. Wnt signaling pathways meet Rho GTPases. Genes. Dev. 23, 265–277.
Schnatwinkel, C., Niswander, L., 2012. Nubp1 is required for lung branching morphogenesis and distal progenitor cell survival in mice. PLoS One 7, e44871.
Schweickert, A., Weber, T., Beyer, T., Vick, P., Bogusch, S., Feistel, K., Blum, M., 2007. Cilia-driven leftward flow determines laterality in xenopus. Curr. Biol.: CB 17, 60–66.
Shahrestanifar, M., Saha, D.P., Scala, L.A., Basu, A., Howells, R.D., 1994. Cloning of a human cDNA encoding a putative nucleotide-binding protein related to *Escherichia coli* MinD. Gene 147, 281–285.
Sive, H.L., Grainger, R.M., Richard, M.H., 2010. Early Development of *Xenopus laevis*: A Laboratory Manual. Cold Spring Harbor Laboratory Press, Cold Spring Harbor.
Skoglund, P., Rolo, A., Chen, X., Gumbiner, B.M., Keller, R., 2008. Convergence and extension at gastrulation require a myosin IIB-dependent cortical actin network. Development 135, 2435–2444.
Smith, J.C., Conlon, F.L., Saka, Y., Tada, M., 2000. Xwnt11 and the regulation of gastrulation in *Xenopus*. Philos. Trans. R Soc. Lond B Biol. Sci. 355, 923–930.
Smith, W.C., Harland, R.M., 1991. Injected Xwnt-8 RNA acts early in *Xenopus* embryos to promote formation of a vegetal dorsalizing center. Cell 67, 753–765.
Sokol, S.Y., 1996. Analysis of Dishevelled signalling pathways during Xenopus development. Curr. Biol. 6, 1456–1467.
Sorokin, S.P., 1968. Reconstructions of centriole formation and ciliogenesis in mammalian lungs. J. Cell Sci. 3, 207–230.
Stehling, O., Netz, D.J., Niggemeyer, B., Rosser, R., Eisenstein, R.S., Puccio, H., Pierik, A.J., Lill, R., 2008. Human Nbp35 is essential for both cytosolic iron-sulfur protein assembly and iron homeostasis. Mol. Cell Biol. 28, 5517–5528.
Steinman, R.M., 1968. An electron microscopic study of ciliogenesis in developing epidermis and trachea in the embryo of *Xenopus laevis*. Am. J. Anat. 122, 19–55.
Stubbs, J.L., Oishi, I., Izpisua Belmonte, J.C., Kintner, C., 2008. The forkhead protein Foxj1 specifies node-like cilia in *Xenopus* and zebrafish embryos. Nat. Genet. 40, 1454–1460.
Tada, M., Smith, J.C., 2000. Xwnt11 is a target of *Xenopus brachyury*: regulation of gastrulation movements via dishevelled, but not through the canonical Wnt pathway. Development 127, 2227–2238.
Tissir, F., Qu, Y., Montcouquiol, M., Zhou, L., Komatsu, K., Shi, D., Fujimori, T., Labeau, J., Tyteca, D., Courtoy, P., Poumay, Y., Uemura, T., Goffinet, A.M., 2010. Lack of cadherins Celsr2 and Celsr3 impairs ependymal ciliogenesis, leading to fatal hydrocephalus. Nat. Neurosci. 13, 700–707.
Vitale, G., Fabre, E., Hurt, E.C., 1996. NBP35 encodes an essential and evolutionary conserved protein in *Saccharomyces cerevisiae* with homology to a superfamily of bacterial ATPases. Gene 178, 97–106.
Wallingford, J.B., 2005. Neural tube closure and neural tube defects: studies in animal models reveal known knowns and known unknowns. Am. J. Med. Genet C Semin. Med. Genet. 135C, 59–68.
Wallingford, J.B., 2006. Planar cell polarity, ciliogenesis and neural tube defects. Hum. Mol. Genet. 15 Spec No 2, R227–234.
Wallingford, J.B., 2010. Planar cell polarity signaling, cilia and polarized ciliary beating. Curr. Opin. Cell Biol. 22, 597–604.
Wallingford, J.B., Fraser, S.E., Harland, R.M., 2002. Convergent extension: the molecular control of polarized cell movement during embryonic development. Dev. Cell 2, 695–706.
Wallingford, J.B., Habas, R., 2005. The developmental biology of Dishevelled: an enigmatic protein governing cell fate and cell polarity. Development 132, 4421–4436.
Wallingford, J.B., Harland, R.M., 2001. *Xenopus* dishevelled signaling regulates both neural and mesodermal convergent extension: parallel forces elongating the body axis. Development 128, 2581–2592.
Wallingford, J.B., Harland, R.M., 2002. Neural tube closure requires dishevelled-dependent convergent extension of the midline. Development 129, 5815–5825.
Wallingford, J.B., Mitchell, B., 2011. Strange as it may seem: the many links between Wnt signaling, planar cell polarity, and cilia. Genes Dev. 25, 201–213.
Wallingford, J.B., Rowning, B.A., Vogeli, K.M., Rothbacher, U., Fraser, S.E., Harland, R. M., 2000. Dishevelled controls cell polarity during *Xenopus* gastrulation. Nature 405, 81–85.
Werner, M.E., Hwang, P., Huisman, F., Taborek, P., Yu, C.C., Mitchell, B.J., 2011. Actin and microtubules drive differential aspects of planar cell polarity in multiciliated cells. J. Cell Biol. 195, 19–26.
Ybot-Gonzalez, P., Savery, D., Gerrelli, D., Signore, M., Mitchell, C.E., Faux, C.H., Greene, N.D., Copp, A.J., 2007. Convergent extension, planar-cell-polarity signalling and initiation of mouse neural tube closure. Development 134, 789–799.
Zariwala, M.A., Knowles, M.R., Omran, H., 2007. Genetic defects in ciliary structure and function. Annu. Rev. Physiol. 69, 423–450.
Zhou, J., Kim, H.Y., Davidson, L.A., 2009. Actomyosin stiffens the vertebrate embryo during crucial stages of elongation and neural tube closure. Development 136, 677–688.